Warming, permafrost thawing and nitrogen availability are drivers of increasing plant growth and species richness on the Tibetan Plateau

Hanbo Yun[1], Qing Zhu[2], Jing Tang[1], Wenxin Zhang[3], Deliang Chen[4], Philippe Ciais[5], Qingbai Wu[6], and Bo Elberling[1]

[1]University of Copenhagen
[2]Lawrence Berkeley National Lab
[3]Lund University
[4]University of Gothenburg
[5]Laboratory for Climate Sciences and the Environment (LSCE)
[6]State Key Laboratory of Frozen Soil Engineering, Northwest Institute of Eco-Environment and Resources, Chinese Academy of Sciences

December 7, 2022

Abstract

Permafrost-affected ecosystems are prone to warming and thawing, which can increase the availability of subsurface nitrogen (N) with consequences for otherwise N-limited tundra vegetation. Here, we show that the upper permafrost of the Tibetan Plateau is subject to thawing and that the upper permafrost zone is rich in ammonium. Furthermore, a five-year ^{15}N tracer experiment showed that long-rooted plant species were able to utilize ^{15}N-labeled N at the permafrost table and far below the main root zone. A 20 years survey is used here to document that long-rooted plant species had a competitive advantage at sites subject to warming and that both plant composition and growth were significantly correlated with permafrost thawing and changes in nitrogen availability. Our experiment documents a clear feedback mechanism of climate warming, which releases plant–available N favoring long-rooted plants and explains important changes in plant composition and growth across sites on the Tibetan Plateau.

Warming, permafrost thawing and nitrogen availability are drivers of increasing plant growth and species richness on the Tibetan Plateau

Hanbo Yun[1,2,3*], Qing Zhu[4], Jing Tang[2,5,6], Wenxin Zhang[2], Deliang Chen[7], Philipp Ciais[8], Qingbai Wu[1*], Bo Elberling[2*]

[1]State Key Laboratory of Frozen Soil Engineering, Beilu'He Observation and Research Station on Tibetan Plateau, Northwest Institute of Eco–Environment and Resources, Chinese Academy of Sciences, 730000 Lanzhou, Gansu, China

[2]Center for Permafrost (CENPERM), University of Copenhagen, DK1350 Copenhagen, Denmark

[3]Department of Earth, Atmospheric, and Planetary Sciences, Purdue University, 47906 West Lafayette, Indiana, USA

[4]Climate Sciences Department, Climate and Ecosystem Sciences Division, Lawrence Berkeley National Laboratory, 94720 Berkeley, California, USA

[5]Department of Physical Geography and Ecosystem Science, Lund University, SE–22236 Lund, Sweden

[6]Department of Biology, Terrestrial Ecology, University of Copenhagen, DK–2100 Copenhagen, Denmark

[7]Department of Earth Sciences, University of Gothenburg, 41320 Gothenburg, Sweden

[8]IPSL – LSCE, CEA CNRS UVSQ UPSaclay, Centre d'Etudes Orme des Merisiers, 91191 Gif sur Yvette France

*Authors for correspondence: Hanbo Yun, hbyun@lzb.ac.cn;

Qingbai Wu, wu@lzb.ac.cn;

Bo Elberling, be@ign.ku.dk

Abstract

Permafrost-affected ecosystems are prone to warming and thawing, which can increase the availability of subsurface nitrogen (N) with consequences for otherwise N-limited tundra vegetation. Here, we show that the upper permafrost of the Tibetan Plateau is subject to thawing and that the upper permafrost zone is rich in ammonium. Furthermore, a five-year ^{15}N tracer experiment showed that long-rooted plant species were able to utilize ^{15}N-labeled N at the permafrost table and far below the main root zone. A 20 years survey is used here to document that long-rooted plant species had a competitive advantage at sites subject to warming and that both plant composition and growth were significantly correlated with permafrost thawing and changes in nitrogen availability. Our experiment documents a clear feedback mechanism of climate warming, which release plant–available N favoring long-rooted plants and explains important changes in plant composition and growth across sites on the Tibetan Plateau.

Keywords

Nitrogen, Permafrost thaw, Climate warming, Tibetan Plateau

1. Introduction

Approximately 25% of the land surface in the Northern Hemisphere is underlain by permafrost (1) and has recently warmed more than twice compared to the rest of the planet (2). This is expected to change both carbon sinks and sources and thereby the resulting net carbon–climate feedback in the tundra ecosystem (3). Tundra plant community composition and plant growth are important components of the carbon budget and have already been shown to change significantly with climate change (4, 5).

The future balance of tundra ecosystem carbon cycles has long been described as being linked to nitrogen (N) cycles, for instance, through thawing permafrost, which can release the N previously held in frozen soil layers (6–8) and thereby change the N availability for plants (9–11) and induce changes in plant growth and plant community composition (12).

Temperature (5, 13), soil moisture (12–15) and nutrition (5, 13, 16, 17) are regarded as central forces causing changes in vegetation composition and plant growth in permafrost-affected ecosystems. However, these factors reveal high spatiotemporal heterogeneity (6, 8, 12), which complicates the understanding and quantification of the mechanisms and drivers of observed changes (5, 17). This is particularly true when scaling observations across permafrost biomes and longer time scales (4, 18).

The Tibetan Plateau accounts for 75% of the Northern Hemisphere's alpine permafrost area and has experienced significant climate and environmental changes in recent decades (19, 20) as well as progressive nitrogen limitation across the Tibetan permafrost region (9). Here, we hypothesized that N released from warmer soils and permafrost thawing is available for long-rooted plant species and that subsequently plant uptake has resulted in changes in plant community composition and growth.

We performed two investigations to quantify the links between permafrost conditions and plant species composition and growth. We first quantified the plant uptake of labeled nitrogen (^{15}N) introduced at the permafrost table for 5 years. Secondly, we repeatedly quantified ambient plant species composition and plant growth based on maximum root depth, plant coverage, plant height and aboveground biomass in September and climate data linked to active layer warming, permafrost thawing and changes in plant availability nutrients. Data were collected from 14 sites across the Tibetan Plateau (Fig. 1) between 1975 and 2017 and included 1838 soil cores from 692 plots and the corresponding plant traits.

2. Methods

Data compilation, quality control and uncertainty analysis. Air temperature, air humidity, soil temperature, soil moisture and total precipitation were obtained from the China Meteorological Data Service Center (http://data.cma.cn/) and the State Key Laboratory of Frozen Soil Engineering, China (SKLFSE; http://sklfse.nieer.ac.cn/; for details, see SI.1.1). The maximum active layer thickness (ALT) was proxied by the maximum thickness of 0 °C for yearly soil temperature. Growing degree days (GDD) were calculated by ref. 27. Soil property data and plant trait data were supported by the SKLFSE, China, and the National Cryosphere Desert Data Center, China (http://www.ncdc.ac.cn/portal/; for details, see Supplementary information (SI.)1.2). Plant species lists (presence/absence data) were made at all sites and plots from 1975, 1978, and 1995–2017 and included 87 species in total. The aboveground biomass in September was quantified from a depth of 1 cm by scissors in three 33 × 33 cm subplots within each 100 × 100 cm plot. The vertical root distribution was based on visually observed fresh roots from the flow water immersion soil core and consisted of three replicates per plot, and the mean value was calculated for the maximum root per plot (SI.1.3). Additional deep soil profile samples were collected in areas with retrogressive thaw slumps near study sites. At these sites, roots were followed to the surface and associated with species-specific living plants and maximum root lengths were recorded (SI.1.3).

The stable isotope ^{15}N data collected from 6 of the above 14 sites belonged to two groups during 2017–2021. At each site, isotopically labeled N (1 g ^{15}N–NH_4Cl, 99 atom%) was dissolved in 50 g deionized water and launched at the permafrost thaw front by a sloping drill hole (Fig. S12). The ^{15}N addition was made in five replicate plots per plant species. Roots at 0–50 cm from three dominant plant species as well as aboveground mass (including leaves and stems) were collected within 33 × 33 cm quarters immediately above the injection point. Collection also included five additional control plots per site, and collection was made approximately ten days, one year, two years, three years and four years after the addition (SI.1.4).

After the above data collections, we conducted data quality control according to ref. 28 (SI.1.5) and uncertainty analysis to 1) examine the spatial autocorrelation in trends in variables related to weather parameters, soil properties and plant traits; and 2) assess whether different location observation years influenced the overall trends (SI.1.6 for details on how we achieved this).

Multiple regression and trend analyses. Stepwise multiple regression analysis was conducted to identify the driver of plant traits (SI.1.13). All variables were standardized by *z*–scores to facilitate comparison of model coefficients across variables with different units. Multicollinearity was checked and was well below ten for all variables (29). The R package leaps was used to select subset models, including all predictors and two–way interactions, and the skill of the model was estimated by the Akaike information criterion (AIC). The results were described by the coefficient (r^2) and p value, significance level <0.05.
We calculated the annual mean values of individual site and group levels for weather parameters, soil properties, soil nutrition and plant traits. The temporal trend of the weather parameter was calculated using the Mann–Kendall test with the R trend package and fitted by the ordinary least–squares method (30). The temporal trends of soil properties, soil nutrients, and plant traits were calculated using linear regression and fitted by the ordinary least–squares method (31). All significance levels were analyzed at $p < 0.05$, and the confidence level was 95%. Datasets were excluded if they were less than 10 years old.

Structure equation model (SEM). Piecewise SEM was examined to identify 1) the pathway of climate change potentially affecting plant growth and 2) the difference between the direct and indirect effects of temperature, water balance and soil nutrition on plant growth. The mean value at the site level for the growing season was used in the SEM analysis and split into two groups, A and B (Fig. S5). Variables that demonstrated a significant correlation (p<0.05) with plant traits in multiple regression analysis were pooled into SEM. Nutrition variation was surrogated by the nitrogen variation, whereas ammonium (NH_4^+) variation delineated the nitrogen released from permafrost (see Supplementary SI.1.14 for justification for this assumption). Ultimately, 7 variables were used in the SEM.

All variables were standardized using *z*–scores (mean zero, unit variance). Then, principal component analysis (PCA) was used to summarize the structure between plant growth and driver parameters. We assumed linear Gaussian relationships between variables included in the model, and we tested for normality with density plots for each variable (32).

As the plant uptake nitrogen released from permafrost has a two-year time lag, the final climate change and plant trait dataset consisted of 1997 to 2017, and the soil nitrogen dataset consisted of 1995 to 2015. We fit separate models window–by–window from 0 to 5 years for growing season and non–growing season to 1) test whether the time lag of 2 years in the SEM was an artifact setting; 2) account for possible time lag effects of climate change variables (i.e., non–growing season air temperature and soil temperature) and nitrogen released from the permafrost thaw front during plant aboveground senescence.

Skill diagnostics. The goodness–of–fit of the SEMs was estimated by the chi–square (x^2), degrees of freedom (*d.f.*), and root–mean–square error of approximation (RMSEA). A path coefficient was used to sign and strengthen the relationships between two variables, which was analogous to the partial correlation coefficient or regression weight (R^2; ref. 33). The standardized total effect was calculated to quantify the contribution of all drivers to plant growth (r^2). The net influence that one variable had upon another was calculated by summing all direct and indirect pathways (effects) between two variables. All SEM analyses were conducted using the piecewiseSEM package of R.

Data Availability. All sites pf soil properties, plant traits data and R code used for the analysis used in this manuscript are publicly available from Electronic Research Data Archive (University of Copenhagen, https://www.erda.dk/), https://sid.erda.dk/sharelink/AMrPDMxk2K.

Acknowledgements. BE and HY were further supported by the Danish National Research Foundation (CENPERM DNRF 100). We thank you Dr. Anping Chen and Prof. Yiqi Luo for suggestion about experiment design and had a level-headed review. We thank you Prof. Yongzhi Liu, Prof. Huijun Jin, Dr. Chao Mao, Guojun Liu, and Guilong Wu for field soil sample processing and laboratory analyses. We also thank Dr. Licheng Liu, and Dr. Youmi Oh for providing assistance with the structure equation model and appreciate Sebastian Zastruzny, Laura Helene Rasmussen, Emily P. Pedersen, Anne Christine Krull Pedersen, and Lena Hermesdorf for providing comments on the data analysis.

More details please see supplementary method.

3. Results

3.1 Climate change on the Tibetan Plateau

Climate data showed that the mean annual air temperature (MAAT) ranged from –4.2 to 0.8 °C from the northern to southern sites across the Tibetan Plateau and significantly increased from the study period 1975 to 2017 ($p < 0.05$; Fig. S1). The annual precipitation ranged from 83 to 460 mm in the study area, and changes over time were noted site specific at few sites (Fig. S2) and mainly during the non-growing season (Figs. S2 a and b).

The mean soil temperature of 0–100 cm was –2.5 ± 1.7 °C, and the mean soil water content (SWC) of 0–100 cm was 12.0 ± 5.3% (Fig. S3). Between 1995 and 2017, the average soil temperatures at 0–100 cm showed different responses at different sites (Fig. S3). The SWC of the 0–100 cm layer did not show significant changes at most sites, except at sites AD and KXL, which showed a significant increase during the study period.

The mean active layer thickness (ALT) of 14 sites measured at the end of the growing season from 1975 to 2017 was 248 ± 38 cm and increased by an average of 20.2 ± 4.6 cm per decade (Fig. S4). A maximum increase in ALT was observed at site QSH (35.8 cm per decade; Fig. S5), which was a relatively dry, well-drained site with low ice content at the top of the permafrost (data not shown). Sites with significant soil warming (0-100 cm) were consistent with the sites with a significant increase in ALT and vice versa for sites without significant soil warming. Based on the observed ALT trends from 1975 to 2017, the 14 study sites were split into group A with significant positive increasing trends, consisting of TSH, QSH, SQH, GZ, MA, WQ, ZAD, XD, ZD, and HSX, and group B without significant changes, consisting of AD and BLH, and with significant negative trends, consisting of KXL and QML (Fig. S5). These two groups were hereafter used for further analyses.

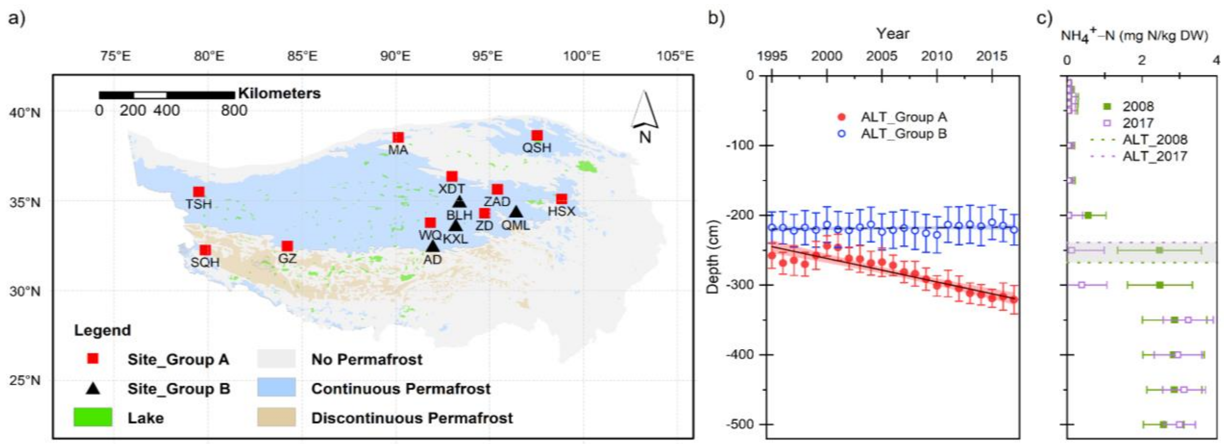

Figure 1. **a**. Map of sampling sites on the Tibetan Plateau (TSH: TianshuiHai; QSH: QingshuiHe; SQH: ShiqianHe; GZ: GaiZi; MA: MangAi; AD: AnDuo; WQ: Wen Quan; KXL: KaixinLing; BLH: BeiluHe basin; ZAD: ZaDuo; XD: XidaTan; ZD: ZhiDuo; QML: QumaLai; HSX: HuashiXia; permafrost distribution by ref. 21, 22). The boundary of the Tibetan Plateau area and permafrost distribution are based on ref. 22. Panel **b** shows the variations in active layer thickness (ALT) from 1995 to 2017 for group A (red solid dot) and group B (blue open circle). A black solid line is a significant change ($p < 0.05$), whereas a black dashed line is not significant ($p > 0.05$). Vertical bars represent one standard deviation, n = 265 for group A and n = 88 for group B. Blue and red ribbons denote the 95% confidence intervals. Panel **c** shows the NH_4^+ profiles of all 14 sites sampled at the end of September 2008 and 2017 (horizontal bars represent one standard deviation, n = 640). Light green and purple dashed lines are the mean thickness of the active layer (ALT) across sites for 2008 and 2017, respectively. The gray region denotes the variation in the permafrost thaw front from 2008 to 2017.

During the study period, on average, 83% of roots were found within the top 50 cm, 16% were within 50–100 cm, and only 1% were below 100 cm. Consequently, the active layer is discussed in the following for each of these three depth intervals (0–50 cm, 50–100 cm, and 100 cm–permafrost table). From 1995 to 2017, the soil bulk density was approximately 1.81 g cm^{-3} for the 0–50 cm, 50–100 cm, and 100 cm–permafrost tables in both group A and group B. The 0–50 cm and 50–100 cm layers showed a significant temporal trend in group A but no significant change in group B. The 100 cm–permafrost table had no temporal trend for both groups A and B (Fig. S6 a and b). A *t*–test showed that the three layers showed no significant difference between groups A and B. Taking the depth–specific soil bulk density and the soil organic carbon (SOC) concentration into account, the SOC stock of 0–50 cm showed a significant decrease (p < 0.01) with a rate of 0.08 ± 0.03 kg C m^{-2} y^{-1} during 1995–2017 in group A (Fig. S7 a). This equals a total C loss of 1.8 kg C m^{-2} over 22 years or that 31% of the SOC within the top 50 cm has been mineralized within the last 20 years. With an average carbon–to–nitrogen ratio (C/N) of 10 (see below), the mineralization is expected to have released on the order of 0.2 kg N m^{-2} over the same period. However, a significant C (or N) loss has not occurred at deeper depth intervals (for group A sites; see Fig. S7 a). For the group B sites, the SOC stock (0–50 cm, 0–100 cm and 0 cm–permafrost table) showed no significant change (Fig. S7 b). Mineralization at 0–50 cm within group A sites did not result in any significant changes in soil pH (Fig. S6 g) or in any other depth intervals with group A or B sites (Fig. S6 h).

The total nitrogen (TN) stock for the group A sites in the upper 0–50 cm layer significantly decreased (p < 0.01), that in the 0–100 cm layer decreased (p = 0.055), and that in the entire active layer (0 cm to permafrost table) significantly increased during 1995–2017 (p < 0.01; Fig. S7 c). For the group B sites, the TN stock of the 0–50 cm, 0–100 cm, and entire active layer did not change significantly (Supplementary Fig. S7 d). The mean carbon–to–nitrogen ratio (C/N) of 0–100 cm was 10.71 ± 2.35 for group A, which significantly increased during 1995–2017 (ranging from 8.82 ± 1.01 to 13.93 ± 1.78; Fig. S7 e), and for group B, the C/N of 0–100 cm was 10.42 ± 1.75 (ranging from 9.52 ± 1.55 to 11.61 ± 2.66), showing no significant change during the same period (Fig. S7 f).

3.2 Release of nitrogen from thawing permafrost and uptake by plants

High-density drilling survey data showed that the ammonium (NH_4^+) extracted from permafrost samples (up to 500 cm below the surface) was approximately 100 times higher than that in samples in the active layer (AL) for both groups A and B from 2008 to 2017 (Fig. 1 c). This result suggests that permafrost thawing can be an important source of NH_4^+ for plant growth if accessible via plant roots (6, 8). This assumption was further explored by an additional ^{15}N experiment.

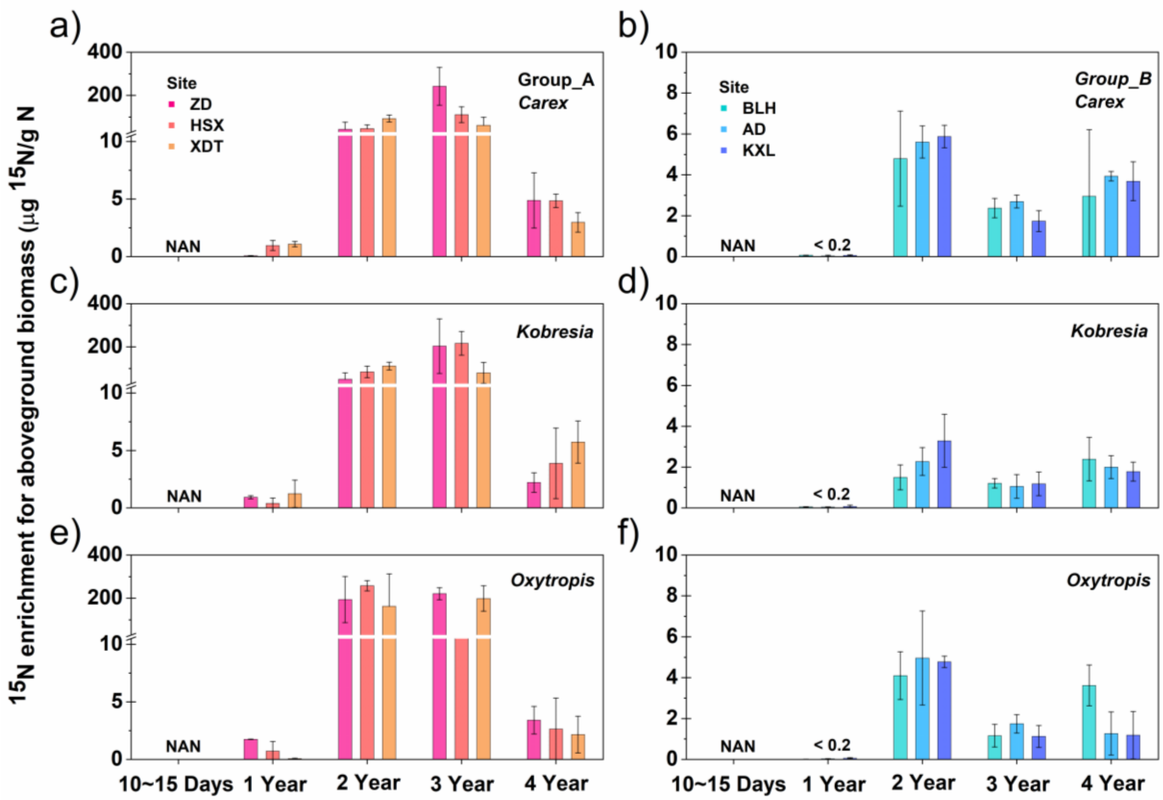

Figure 2. Enrichment $^{15}N\_NH_4$ in aboveground biomass (including leaves and stem) of long-root species (average root length between 35 to 55 cm) by treatment after 10~15 days, 1 year, 2 years, 3 years, and 4 years for group A (**a**, **c**, **e**) and group B (**b**, **d**, **f**). **a** and **b** are *Carex moorcroftii* Falc. Ex Boott (*Carex*), **c** and **d** are *Kobresia littledalei* C. B. Clarke (*Kobresia*), and **e** and **f** are *Oxytropis pauciflora* Bunge (*Oxytropis*). Vertical bars represent one standard deviation, n = 15 (after 1 year, n= 12).

To explore whether NH_4^+ released at the permafrost table in autumn is accessible to plants, a stable isotopic labeling ($^{15}N–NH_4^+$) experiment was conducted during 2017–2021. The investigation included both long-root species (root length ≥ 20 cm; Fig. 2) and shallow-root species (root length < 20 cm; Fig. S8). Our results showed that at one year after addition, plant aboveground tissue had a significant amount of labeled N (Fig. 2). This result suggests that roots can utilize N at an average depth of 3.3 m below the surface (mean thickness of the maximum active layer) and even as deep as 3.6 m below the surface at site XD, which corresponding to the maximum active layer thickness and deepest injection depth. This is far deeper than previously reported for the Arctic (23–26) and is critical for plants living on the Tibetan Plateau. In this study, the recorded mean root depth was 24.1 ± 16.3 cm (ranging from 2.7 ± 1.2 to 103.7 ± 17.4 cm; Table S1), which was rather shallow compared with the mean ATL (248 ± 38 cm; Fig. S4). This highlights that only a few long roots are important for utilizing deep permafrost-released N. In the addition $^{15}N–NH_4^+$ experiment, nitrogen was supplied only as ammonium; however, because ammonium can be converted to nitrate through nitrification, it was not possible to conclude if plants incorporated permafrost N as ammonium or nitrate in here. The observations highlight the potential of long-rooted species benefitting from permafrost-released N compared more than shallow-rooted species.

3.3 The link between nitrogen dynamics and plant growth

Long-term trends in biologically available N and plant traits were used to assess the links between climate change-driven N dynamics and plant growth. There were 85 graminoids and 2 dwarf deciduous shrubs (*Potentilla parvifolia* Fisch. ex. Lehm. and *Myricaria prostrata* Hook. f. et Thoms. ex Benth.) recorded in group A (Table ST1), and the mean species richness increased from 15.5 species per m^2 (1995) to 23.8 species per m^2 (2010; $p < 0.1$) and then declined to 18.5 species per m^2 (2017; $p < 0.05$; Fig. S9 a). There were 62 graminoid species and one dwarf deciduous shrub (*Myricaria prostrata* Hook. f. et Thoms. ex Benth.) in group B (Table ST2), and no temporal trends were observed (with a mean species richness of 16.1 per m^2; Supplementary Fig. S9 b). From 1975–2017, the maximum root depth significantly increased from 66.8 ± 15.2 to 103.7 ± 17.4 cm in group A (Tables ST1), during which no significant change (from 62.7 ± 6.7 to 75.6 ± 5.1 cm) was noted for group B (Tables ST2). Specific species root traits were not sampled for all known plant species during the study period. However, the maximum root depths of four plant species known to have long roots were quantified in selected sites in both groups A and B (Fig. 3). For these four plant species, the maximum root depth increased significantly. For instance, *Astragalus melanostachys* roots changed from 52.1 ± 5.9 cm in 1995 to 69.7 ± 5.3 cm in 2017 at group A sites, but no significant change was observed at group B sites (Fig. 3c).

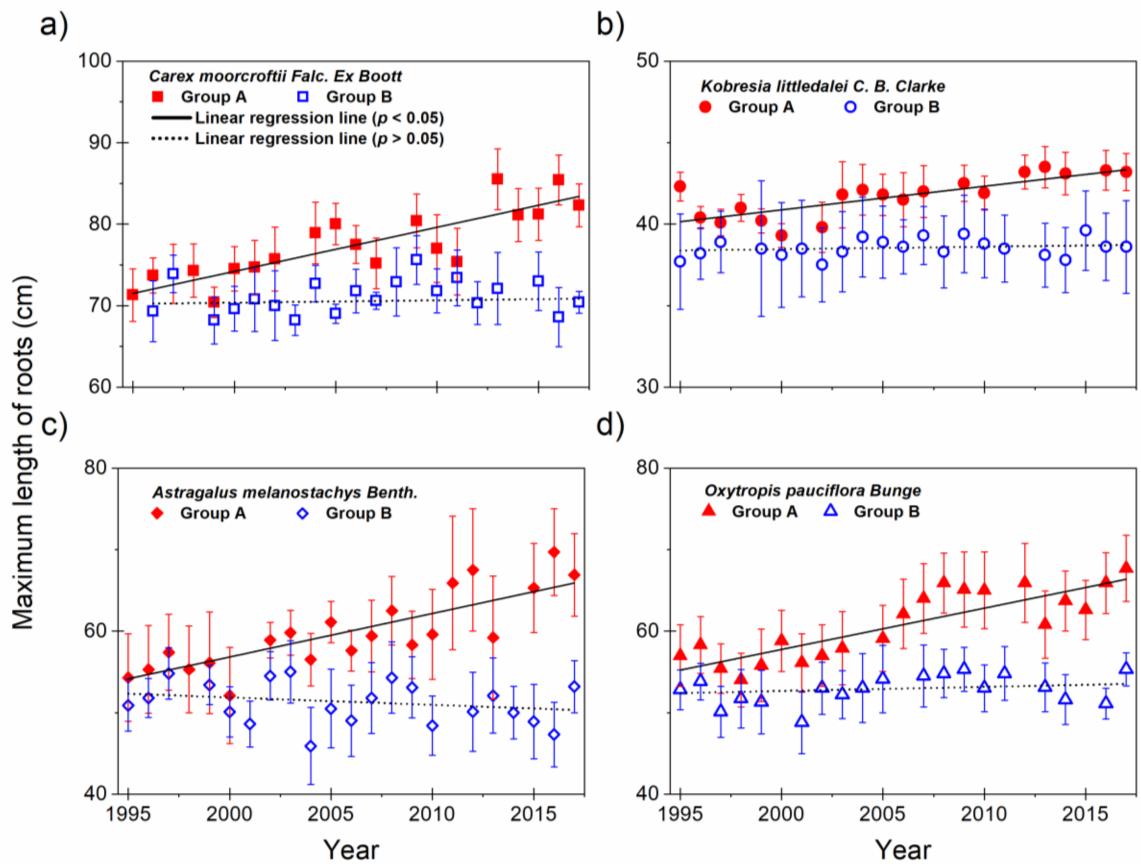

Fig. 3 Changes in maximum length of plant-specific roots for four long-rooted species for group A and group B sites from 1995 to 2017. **a** is *Carex moorcroftii* Falc. Ex Boott, **b** is *Kobresia littledalei* C. B. Clarke*,* **c** is *Astragalus melanostachys* Benth.*,* and **d** is *Oxytropis pauciflora* Bunge. Vertical bars represent one standard deviation, n = 4.

At group A sites with significant permafrost thawing and active layer warming, long-rooted plant species had significantly increased root length and were able to utilize added ^{15}N at the permafrost table. Furthermore, root sampling at retrogressive thaw slumps reveled species-specific roots at least 2.4 m below the surface related to *Kobresia littledalei* C. B. Clarke and *Oxytropis pauciflora* Bunge (see SI.1.3).

The above observations show that long-rooted species have been able to utilize additional N from soils below the main root zone and suggest that N-derived from permafrost thawing can influence plant composition and plant growth. In particular, long-rooted plant species seem to have an advantage when nutrients and water are limited. This result is aligned with that in group A sites, which showed a clear relationship between the vertical maximum root depth increase ($p < 0.01$) and the species composition change, while this was, as expected, not observed for group B sites (Fig. S9). Furthermore, convergent crossing mapping (CCM) was conducted between variations in the maximum root length and variations in the nitrogen of 50–100 cm, which had a positive correlation during 1995–2017. The CCM results showed that the direct impacts of variations in nitrogen of 50–100 cm drove the variations in maximum root length and not that root growth affected nitrogen at 50–100 cm (Fig. S10).

Subsequently, we compared the aboveground biomass in September between group A and group B from 1995 to 2017 (Table ST3). The mean aboveground biomass in September was 234.5 ± 8.0 g per m^2 for group A and 249.4 ± 6.9 g per m^2 for group B. Although the *t*–test revealed no significant differences between group A and group B, the aboveground biomass at group A sites increased significantly during 1995–2002 ($p < 0.05$) but decreased significantly during 2003–2012 ($p < 0.01$; Table ST3). For group B, the aboveground biomass did not show any significant change in either subperiod.

Interestingly, from 2008 to 2020 at permafrost thawing sites (group A), the plant species-specific results showed no consistent pattern of root length increase or biomass accumulation, either aboveground or belowground, e.g., at site XD (Fig. S11). For the species with long roots, *Anemone imbricata* Maxim. and *Oxytropis glacialis*, root length increased significantly as aboveground biomass increased, while the shallow-root species of *Leontopodium pusillum* (Beauv.) Hand.–Mazz. and *Heteropappus bowerii* (Hemsl.) Griers. showed no changes in root length or aboveground biomass. Furthermore, the root length of *Saussurea wellbyi* Hemsl. decreased significantly, while aboveground biomass increased significantly. This result suggests that shallow-root species can be affected differently by climate change than long-root species on the Tibetan Plateau. Shallow-root species may benefit from near–surface increasing mineralization linked to AL warming, while long-root species significantly increased in both root length and aboveground biomass, which could be due to the increased N availability linked to permafrost thawing.

4. Discussion

4.1 Pathway between climate change and plant community composition

To examine pathways by which climate change potentially affects plant growth and to differentiate between direct and indirect effects of temperature (air temperature, growing degree days, soil temperature of 0–50 cm, soil temperature of 50–100 cm, variation -of ALT), water balance (soil moisture of 0–50 cm, soil moisture of 50–100 cm) and soil nutrition (N–NO_3^- and N–NH_4^+ concentration for 0–50 cm, 50–100 cm, 100 cm–permafrost front table) on plant growth, we used piecewise structural equation models (SEMs). The SEM (Fig. 4) highlighted the importance of the maximum root length (R^2=0.76) on plant growth, rather than the importance of the growing degree days (R^2=0.59) and active layer warming (R^2=0.59). The change in the maximum length of the root was roughly equally controlled by the active layer warming (R^2=0.66) and permafrost thawing (R^2=0.68).

Alleged with the additional ^{15}N experimental results, the SEM results implied that long-rooted species will benefit from AL warming and permafrost thawing, while shallow-rooted species benefit mainly from GDD. Overall, 72% of plant growth could be explained by the maximum root depth, AL warming, and GDD together, whereas 69% of the variation in the maximum root depth could be explained by AL warming and permafrost thawing alone(Fig. 4). This suggests that plant species composition in the future may depend on how different species benefit from near-surface warming versus permafrost thawing. More than 1/3 of the near–surface organic carbon has been mineralized, probably due to climate warming, which has resulted in a major near–surface inorganic N source. However, the N source linked to the permafrost table was more complex and may be available directly for plants as NH_4^+ (or NO_3^- after nitrification).

Vegetation composition changes and root dynamics in permafrost regions have important implications for ecosystem C cycling (23). The increases in root length, root exudates, and litter input may provide more C and N under warmer conditions (8, 23) as well as more N released from the permafrost table (6). The marked increase in the SOC content of the 50–100 cm layer and the change in the C/N ratio at group A sites suggest that changes in vertical root distribution could lead to additional root litter in the 50–100 cm layer and thereby explain an increase in SOC.

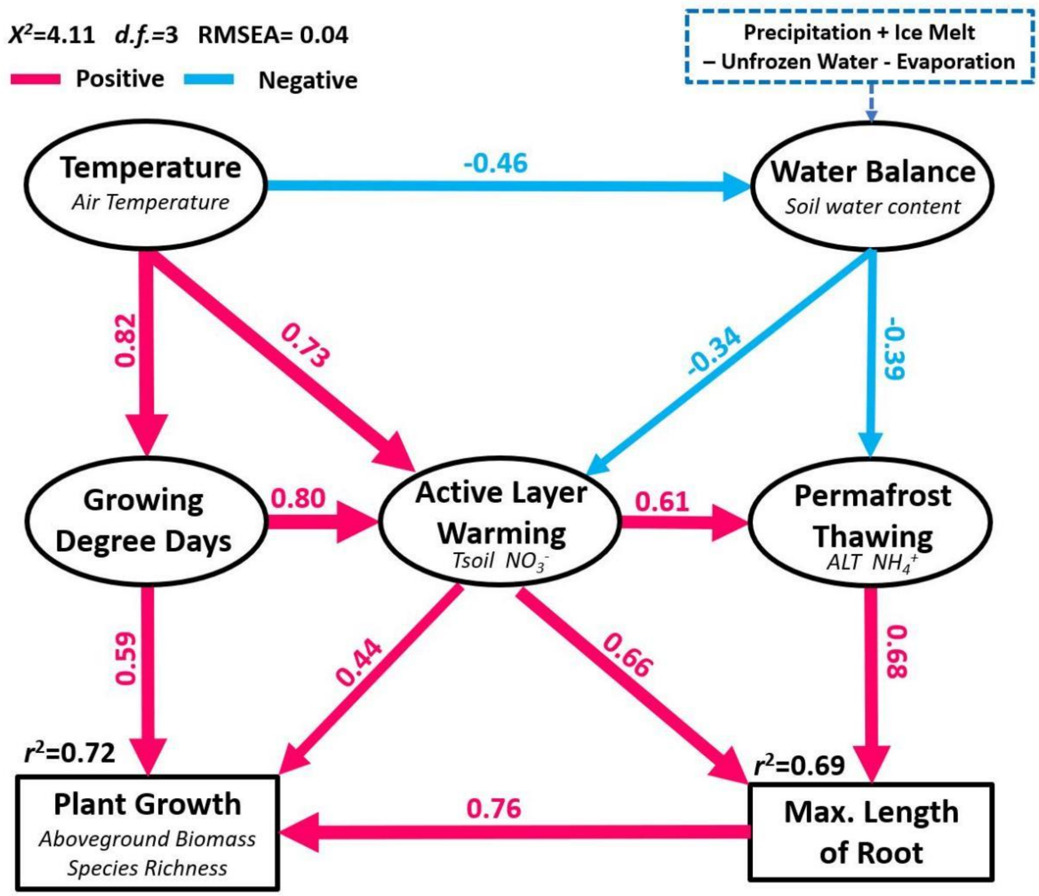

Figure 4. The structural equation model (SEM) quantifies the direct and indirect pathways of climate change on ecosystem changes measured as plant growth through additional nitrogen availability due to either active layer warming or permafrost thawing based on data from group A sites during 1995–2017. The numbers shown by the arrows are the standardized path coefficients and indicate the effect size of the relationship between two variables. Arrow widths are proportional to the path coefficient values. Only significant relationships are shown ($p < 0.05$). Red and blue arrows indicate positive and negative relationships, respectively. The chi–square statistic (χ^2), degrees of freedom (*d.f.*) and the root–mean–square error of approximation (RMSEA) are shown in the left–upper corner of the figure. For more details, please see Supplementary SI.1.14.

We conclude that (1) the permafrost layer contains higher levels of ammonium than the active layer, and ammonium is released upon thawing (nitrate can be produced in these aerated soil systems by nitrification); (2) active layer warming has resulted in corresponding enhanced soil organic matter mineralization within the top 50 cm, and permafrost thawing with corresponding released ammonium are two important sources of inorganic nitrogen, which together is attributed to significant changes in species composition and plant growth; (3) increasing nitrogen levels corresponded to an increase in root growth and changes in plant species composition; and (4) SEM analysis indicated that climate affected plant growth (including directly and indirectly), which explained 69% of the variation in maximum root depth and 72% of the variation in plant growth. Plant variation was associated with indirect processes controlled by permafrost thawing and the associated release of plant nutrients or other factors.

In summary, climate warming has led to both warming of the AL and significant thawing of the permafrost in 10 of 14 sites across the Tibetan Plateau during the past four decades. These changes have increased the subsurface nitrogen availability from the soil surface to the permafrost table. Labeled ammonium addition (^{15}N), repeated field drilling, plant survey and SEM analysis revealed the linkage between the availability of nitrogen and a significant increase in the maximum root depth and suggested that long-rooted plant species benefitted from deeper nitrogen sources and affected species composition and aboveground plant growth. While we did not observe a significant change in aboveground biomass carbon storage at the four-decade scale, the strong trend of changing plant community composition may have important implications for biophysical feedbacks to the climate. Although this cascading biophysical effect requires further research, our findings highlight the complex interactions among climate, permafrost, nutrient cycling, and vegetation dynamics that could have lasting impacts on the ecosystem and the people of the world's highest land.

Data Availability

All sites pf soil properties, plant traits data and R code used for the analysis used in this manuscript are publicly available from Electronic Research Data Archive (University of Copenhagen, https://www.erda.dk/), https://sid.erda.dk/sharelink/AMrPDMxk2K.

Author contributions.

H.B. Yun, Q.B. Wu and B. Elberling designed project and wrote the manuscript with contributions from all authors. H.B. Yun, B. Elberling, Q. Zhu, J. Tang, W.X. Zhang and D.L. Chen performed data analysis. P. Ciais reviewed the manuscript. H.B. Yun and Q.B. Wu collected in-situ data and finished measurements in the lab.

Competing interests.

The contact author has declared that none of the authors has any competing interests.

Acknowledgements

BE and HY were further supported by the Danish National Research Foundation (CENPERM DNRF 100). We thank you Dr. Anping Chen and Prof. Yiqi Luo for suggestion about experiment design and had a level-headed review. We thank you Prof. Yongzhi Liu, Prof. Huijun Jin, Dr. Chao Mao, Guojun Liu, and Guilong Wu for field soil sample processing and laboratory analyses. We also thank Dr. Licheng Liu, and Dr. Youmi Oh for providing assistance with the structure equation model and appreciate Sebastian Zastruzny, Laura Helene Rasmussen, Emily P. Pedersen, Anne Christine Krull Pedersen, and Lena Hermesdorf for providing comments on the data analysis.

References

1. Obu, J., et al., Northern Hemisphere permafrost map based on TTOP modelling for 2000–2016 at 1 km2 scale. *Earth Sci. Rev.*, *193*, 299-316 (2019). https://doi.org/10.1016/j.earscirev.2019.04.023
2. Parmesan, C., et al., Terrestrial and Freshwater Ecosystems and their Services. In: *Climate Change 2022: Impacts, Adaptation, and Vulnerability.* Contribution of Working Group II to the Sixth Assessment Report of the Intergovernmental Panel on Climate Change [H.-O. Pörtner, et al., (eds.)]. Cambridge University Press. In Press (2022). https://doi.org/10.5194/bg-11-6573-2014
3. Virkkala, A. M., et al., Statistical upscaling of ecosystem CO2 fluxes across the terrestrial tundra and boreal domain: Regional patterns and uncertainties. *Glob. Chang. Biol.*, *27*(17), 4040-4059(2021). https://doi.org/10.1111/gcb.15659
4. Bjorkman, A. D., et al., Plant functional trait change across a warming tundra biome. *Nat.*, *562*(7725), 57-62(2018). https://doi.org/10.1038/s41586-018-0563-7
5. Niittynen, P., Heikkinen, R. K., & Luoto, M., Snow cover is a neglected driver of Arctic biodiversity loss. *Nat. Clim. Chang.*, *8*(11), 997-1001(2018). https://doi.org/10.1038/s41558-018-0311-x
6. Elberling, B., Christiansen, H. H., & Hansen, B. U., High nitrous oxide production from thawing permafrost. *Nat. Geosci.*, *3*(5), 332-335(2010). https://doi.org/10.1038/ngeo803
7. Keuper, F., et al., Experimentally increased nutrient availability at the permafrost thaw front selectively enhances biomass production of deep-rooting subarctic peatland species. *Glob. Chang. Biol.*, *23*(10), 4257-4266 (2017). https://doi.org/10.1111/gcb.13804
8. Salmon, V. G., et al., Adding depth to our understanding of nitrogen dynamics in permafrost soils. *J. Geophys. Res. Biogeosci.*, *123*(8), 2497-2512(2018).

https://doi.org/10.1029/2018JG004518

9. Kou, D., et al., Progressive nitrogen limitation across the Tibetan alpine permafrost region. *Nature communications*, 11(1), 1-9 (2020). https://doi.org/10.1038/s41467-020-17169-6
10. Hewitt, R. E., Taylor, D. L., Genet, H., McGuire, A. D., & Mack, M. C. Below-ground plant traits influence tundra plant acquisition of newly thawed permafrost nitrogen. *J. Ecol.*, *107*(2), 950-962(2019). https://doi.org/10.1111/1365-2745.13062
11. Pedersen, E. P., Elberling, B., & Michelsen, A. Foraging deeply: Depth-specific plant nitrogen uptake in response to climate-induced N-release and permafrost thaw in the High Arctic. *Glob. Chang. Biol.*, *26*(11), 6523-6536(2020). https://doi.org/10.1111/gcb.15306
12. Heijmans, M. M., et al., Tundra vegetation change and impacts on permafrost. *Nat. Rev. Earth Environ.*, *3*(1), 68-84(2022). https://doi.org/10.1038/s43017-021-00233-0
13. Elmendorf, S. C., et al., Plot-scale evidence of tundra vegetation change and links to recent summer warming. *Nat. clim. Chang.*, 2(6), 453-457(2012). https://doi.org/10.1038/nclimate1465
14. Kemppinen, J., Soil moisture and its importance for tundra plants (2020). http://urn.fi/URN:ISBN:978-951-51-4933-6
15. Happonen, K., Virkkala, A. M., Kemppinen, J., Niittynen, P., & Luoto, M., Relationships between above‐ground plant traits and carbon cycling in tundra plant communities. *J. Ecol.*, 110(3), 700-716(2022). https://doi.org/10.1111/1365-2745.13832
16. Schuur, E. A., Crummer, K. G., Vogel, J. G., & Mack, M. C., Plant species composition and productivity following permafrost thaw and thermokarst in Alaskan tundra. *Ecosyst.*, *10*(2), 280-292(2007). https://doi.org/10.1007/s10021-007-9024-0

17. Myers-Smith, I. H., et al., Eighteen years of ecological monitoring reveals multiple lines of evidence for tundra vegetation change. *Ecol. Monogr.*, *89*(2), e01351(2019). https://doi.org/10.1002/ecm.1351

18. Thomas, H. J., et al., Global plant trait relationships extend to the climatic extremes of the tundra biome. *Nat. Commun.*, *11*(1), 1-12(2020). https://doi.org/10.1038/s41467-020-15014-4

19. Chen, D., et al., Assessment of past, present and future environmental changes on the Tibetan Plateau. *Chin. Sci. Bull*., 60(32), 3025-3035(2015). https://doi.org/10.1360/N972014-01370

20. Yao, T., et al., Recent third pole's rapid warming accompanies cryospheric melt and water cycle intensification and interactions between monsoon and environment: Multidisciplinary approach with observations, modelling, and analysis. *Bull. Am. Meteorol. Soc.*, 100(3), 423-444(2019). https://doi.org/10.1175/BAMS-D-17-0057.1

21. Wang, T., et al., Permafrost thawing puts the frozen carbon at risk over the Tibetan Plateau. *Sci. Adv.*, 6(19), eaaz3513(2020). https://doi.org/10.1126/sciadv.aaz3513

22. Zou, D., et al., A new map of permafrost distribution on the Tibetan Plateau. *Cryosphere*, *11*(6), 2527-2542(2017). https://doi.org/10.5194/tc-11-2527-2017

23. Blume-Werry, G., Milbau, A., Teuber, L. M., Johansson, M., & Dorrepaal, E., Dwelling in the deep–strongly increased root growth and rooting depth enhance plant interactions with thawing permafrost soil. *New Phytol.*, *223*(3), 1328-1339(2019). https://doi.org/10.1111/nph.15903

24. Finger, R. A., et al., Effects of permafrost thaw on nitrogen availability and plant–soil interactions in a boreal Alaskan lowland. *J. Ecol.*, *104*(6), 1542-1554(2016). https://doi.org/10.1111/1365-2745.12639

25. Abramoff, R. Z., & Finzi, A. C., Are above-and below-ground phenology in sync?. *New Phytol.*, *205*(3), 1054-1061(2015). https://doi.org/10.1111/nph.13111

26. Riley, W. J., Zhu, Q., & Tang, J. Y., Weaker land–climate feedbacks from nutrient uptake during photosynthesis-inactive periods. *Nat. Clim. Chang.*, *8*(11), 1002-1006(2018). https://doi.org/10.1038/s41558-018-0325-4

27. Bendixen, M., et al., Delta progradation in Greenland driven by increasing glacial mass loss. *Nat.*, *550*(7674), 101-104. (2017). https://doi.org/10.1038/nature23873

28. Essington, T., et al., Historical reconstruction of the Puget Sound (USA) groundfish community. *Mar. Ecol. Prog. Ser.*, 657, 173-189(2021). https://doi.org/10.3354/meps13547

29. Queen, J. P., Quinn, G. P., & Keough, M. J., *Experimental design and data analysis for biologists*. Cambridge university press (2002).

30. Essington, T. E., *Introduction to Quantitative Ecology: Mathematical and Statistical Modelling for Beginners*. Oxford University Press (2021).

31. Pinheiro, J. C., & Bates, D. M., Linear mixed-effects models: basic concepts and examples. Mixed-effects models in S and S-Plus, Statistics and Computing. Springer, 3-56(2000). https://doi.org/10.1007/0-387-22747-4_1

32. Grace, J. B., Structural equation modeling and natural systems. Cambridge University Press (2006).

33. Mallet, A. A., A maximum likelihood estimation method for random coefficient regression models. *Biometrika*, 73(3), 645-656(1986). https://doi.org/10.1093/biomet/73.3.645

Supplementary information

SI.1 Methods

SI.1.1 Meteorological data compilation

QML(QumaLai), TSH (TianshuiHai), SQH (ShiquanHe), ZD (ZhiDuo), MA (MangAi), GZ (GaiZe), WQ (WenQuan), QSH (QingshuiHe), and ZAD (ZaDuo) can be downloaded from the meteorological data service center, China (http://data.cma.cn/), whereas BLH (Beilu'He), KXL (Kaixinling), AD (Anduo), XD(XidaTan), and HSX(HuashiXia) were provided by the State Key Laboratory of Frozen Soil Engineering (SKLFSE), China (http://sklfse.nieer.ac.cn/). The approach to address the data gaps is described in ref. 1 and 2. We used linear interpolation to address the dataset gaps if they were less than 2 hours, and we used a method described in ref. 3 to address gaps greater than 2 hours but less than 1 day. Furthermore, we used an artificial neural network approach as described in ref. 4 to fill gaps greater than 1 day.

Air temperature was measured by a 2 m tower, and the air temperature sensor was GB10589–89 (Yueke, Chengdu, China). In addition, during 1995–2002, the air sensor was HMP45C (Campbell, Logan, UT 84321–1784, USA), and from 2003 to 2017, the sensor was replaced by HMP155A (Campbell, Logan, UT 84321–1784, USA). From 1975 to 2002, precipitation data were measured by ZGQX–95 (Zhongguoqixiang, Beijing, China), and from 2003 to 2017, precipitation data were measured by T200B (Geonor, Oslo, Norway).

Soil temperatures in the 0–50 cm and 50–100 cm soil layers prior to 1990 were measured manually once or twice per month using a mercury thermometer (with an accuracy of $\pm$ 0.2 °C). From 1990, all soil temperatures were measured using a string of thermistors made by the SKLFSE (Lanzhou, China). The soil water contents (SWCs) of the 0–50 cm and 50–100 cm soil layers prior to 1995 were calculated gravimetrically using the ratio of the water mass present to the oven–dried (75 °C, 24 hours) weight of the soil sample 1~3 times per year. Since 1995, SWC has been measured by a pF–meter sensor (GEO–Precision, Environmental Industry Companies, Ettlingen, D-76275, Germany).

All the above data obtained by the different sensors were calibrated by the Meteorological Data Service Center of the SKLFSE, China.

Following Muller's original definition, the maximum active layer thickness (ALT) is the maximum thawing depth in late autumn using a linear interpolation of the temperature of soil profiles between two neighboring points above and below the 0 °C isotherm, as previously described (5).

Growing degree day (GDD) is often used to quantify temperature or heat requirements for plant development and is the cumulative sum of air temperatures above a certain degree. GDD is a heuristic tool in phenology that is widely used in mechanism–based phenological models (6). Here, GDD is calculated as the cumulative sum of daily air temperatures above 0 °C following ref. 7.

SI.1.2 Soil property data compilation

All soil cores were taken as two pseudoreplicate cores within 0.5° × 0.5° (latitude and longitude) and from the same vegetation type. The nine locations (AD, QML, BLH, HSX, TSH, SQH, ZD, MA, and GZ) had 62 plots and 1078 cores that were studied in 1975 and 1978 and from 1995 to 2017 (26 years). The 5 locations of WQ, QSH, KXL, ZAD and XD had a total of 96 plots and 760 cores, which were studied from 2002 to 2017 (16 years).

For each soil core, samples from 0–100 cm were collected by a soil corer (diameter is 5 cm) at 0–5 cm, 5–10 cm, 10–15 cm, 15–20 cm, 20–30 cm, 30–40 cm, 40–50 cm, 50–100 cm, and for the soil between 100 cm to 500 or 550 cm, we used a motorized drill to collect the samples at 50 cm intervals. The samples were collected using a stainless steel ring cutter, with three replicates. The permafrost table was determined by the ice content of the core sampling (5, 8). Near the permafrost table, we collected soil samples every 5 cm in the upper and lower 50 cm ranges. All samples were marked and sealed in a 100 ml steel aluminum box, weighed, frozen at –15 °C, and brought back to the laboratory used for soil property analysis.

Soil pH was determined by amperometry (DJS–1C, Leizi, Shanghai, China). Five grams of fresh soil was mixed with $CaCl_2$ (0.2 M) at a ratio of 1 part soil to 5 parts liquid, and then, the pH of the suspension was measured after 1 hour of shaking for each soil sample of a given year.

Soil bulk density was calculated based on total fresh weight, soil water content and total soil volume.

Soil organic carbon (SOC) of the air-dried soil samples was analyzed using the wet combustion method, Walkley–Black modified acid dichromate digestion, $FeSO_4$ titration, and an automatic titrator (9, 10).

Total nitrogen (TN) was titrated by the Kjeldahl method (Wu et al., 2016) before 2000, and since 2001, it has been measured by an elementary analyzer (Vario EL Three, Elementar, Germany). All the data transitions between the Kjeldahl method and elemental auto–analysis followed the method described in the lecture of the Chinese ecosystem research network (http://cern.ac.cn).

The ratio between soil carbon and nitrogen (C:N) was then calculated as the quotient of the SOC and TN concentrations.

Chloride (Cl^-) was measured by $AgNO_3$ titration. Calcium (Ca^{2+}) and magnesium (Mg^{2+}) were measured by EDTA titration. Sodium (Na^+) was measured by a blaze photometer (FP6400, JINGMI, Shanghai, China). For more details of the methods, please see the Chinese ecosystem research network, China (http://cern.ac.cn), and for primary results, please see Fig. S13

Nitrate ($N–NO_3^-$) was measured by capacity titration (ELIT 8021, Beijing, China) prior to 2000; since 2001, ion chromatography (T6–New Century Spectrophotometer, PUXI, Beijing, China) has been used. The NO_3^- data obtained by the different methods were calibrated by the SKLFSE, China.

Ammonium ($N–NH_4^+$) was analyzed based on soil samples (2008–2017) with the initial moisture content. The soil samples were extracted by 2 M KCl and then quantified using a flow injection analyzer (Autoanalyzer 3 SEAL, Bran and Luebbe, Norderstedt, Germany), and the limit of detection was 0.003 N mg L^{-1}. The NH_4^+ concentration was subsequently calculated as mg N kg^{-1} dry weight (DW) of soil.

SI.1.3 Plant trait data compilation

For each plot, species identification, vegetation height, landscape types, characteristics of surface drainage and erosion status were recorded. Plant coverage was measured in the early or middle of September at 5 plots (1 m × 1 m) placed with a 500 m radius of the borehole position. In 1975 and 1978, it was measured based observations by experts. From 1995 to 2007, using the pin-point method, a 10 cm × 10 cm nylon mesh was laid in a 1 m × 1 m plot to estimate the plant coverage. From 2008 to 2017, a US agricultural multispectral camera was used to measure the plant coverage. The difference in plant coverage between the different methods was successfully validated by linear regression (r^2>0.9.)

Plant height was measured by a 10-point frame sample (wind speed < 0.5 m/s). Forty-five degrees slowly downward from the pin, when the pin first hit the target grass leaf, was recorded and calculated as the individual plant height, with 5 repeats. The average of 50 samples (10 points × 5 repeats) was recorded as the plant height. Finally, the mean height for the plot was calculated for any given year.

The aboveground biomass in September was quantified in three 20 cm × 20 cm subplots within each plot during September, for a total of 15 subplots per site. At each subplot, aboveground biomass was cut using scissors, packed in paper bags and returned to the laboratory, where all samples were filtered through a 1 mm × 1 mm sieve to remove soil, and plant samples were dried at 75 ± 2 °C for 72 hours to calculate the aboveground biomass.

To investigate the root vertical distribution pattern of the plant species in the community, a 1.5 m depth pit was dug in five 1.5 m × 1.5 m quadrats to measure the maximum root depth after all of the above work was finished. Since 2008, this approach has been replaced by a special soil sample drill device (diameter is 15 cm) designed by SKLFSE, China.

The vertical root distribution was based on visually observed fresh roots from the flow water immersion soil core and consisted of three replicates per plot. A mean value was calculated for the maximum root per plot.

Additional deep soil profile samples were collected in areas with retrogressive thaw slumps near study sites. Non of the actual study sites reveal such features. At these sites, roots were followed to the surface and associated with species-specific living plants. Maximum root lengths which could be linked to individual plants were recorded.

The photo shows a retrogressive thaw slump. Thawing permafrost and a collapsed landscape has exposed soil profiles to a depth of about 5 m. The main root zone was within the upper 0.5 m and the active layer depth 2.8 m. Species-specific roots were found at least 2.4 m below the surface (shown with an yellow dashed line) and related to *Kobresia littledalei* C. B. Clarke and *Oxytropis pauciflora* Bunge. The location is 55 km North of ZAD (ZaDuo) and described July 13, 2021.

SI.1.4 Stable isotope ^{15}N data compilation

To quantify if the ammonium released during permafrost thawing can be taken up by plants, 210 plots (including 30 control plots) of 6 sites for both group A (ZD, HSX, and XDT) and group B (BLH, AD, and KXL) were set on 5th to 18th September 2017, which is close to the time of maximum active layer depth and corresponds to the end of the aboveground growing season and onset of plant senescence. N release from the permafrost was mimicked by injecting a trace amount of the stable isotope ^{15}N into the soil at the depth of the thawing permafrost front. At each plot isotopically labeled N, 1 g $^{15}N\text{-}NH_4Cl$, 99 atom%, was dissolved in 50 g deionized water and wrapped in polyvinyl chloride capsule. To avoid interruption to the ground surface environment, a capsule was launched into the thawing permafrost front by a hallow, narrow slope steel drill (Supplementary Fig. S12), and then, a radar (precise: 0.02 m for 500 MHz; MALA ProEx, MALA, Sweden) was used to confirm the location of the capsule and plant sample plot.

To assess the time-scale of isotope nitrogen uptake by plants, the dominant plant roots of the 0-50 cm soil layer and aboveground mass (including leaves and stems) were collected within 33×33 cm quarters immediately above the capsule after treatment for 10~15 days, one year, two years, three years and four years. There were six primary dominant species at 6 sites, including 3 deep-rooted species, which were *Carex moorcroftii Falc*. Ex Boott (*Carex*), *Kobresia tibetica* Maxim. (*Kobresia*), and *Oxytropis* glacialis (*Oxytropis*), and 3 shallow-rooted species, which were *Heteropappus bowerii* (Hemsl.) Griers. *(Heteropappus), Leontopodium nanum (Hook. f. et Thoms.) Hand.-Ma* (Leontopodium), and *Saussurea arenaria* Maxim (*Saussurea*). It was not possible to macroscopically separate roots for all plant species, but species could be sorted as deep-rooted and shallow-rooted plant species by hand.

The stable isotope ^{15}N is naturally present in very low quantities in plants. By adding a trace amount of ^{15}N, N uptake can be measured by determining the excess ^{15}N content compared to the naturally occurring ^{15}N found in the total N pool. Thus, excess ^{15}N, or ^{15}N enrichment, was calculated as the difference in atom% ^{15}N between the samples from the treated (isotopically labeled) and untreated (natural abundance) plots:

$$atom\%_{excess} = atom\%_{sample} - atom\%_{nature\ abundance}$$

Atom% is calculated as:

$$atom\% = \frac{100 \times (\delta + 1{,}000)}{\delta + 1{,}000 + \frac{1{,}000}{R_{st}}}$$

where δ is the $\delta^{15}N$ for the sample (‰), and R_{st} is the 15N/14N ratio of the international reference material (0.003676). Samples with naturally abundant $\delta\ ^{15}N$ were collected from the untreated plots at specific species and harvest times. In this study, potential seasonal changes in the natural abundance of $\delta\ ^{15}N$ in plants and the significant levels of isotopic enrichment showed that the potential temporal variation in $\delta^{15}N$ was negligible. Excess ^{15}N is expressed as the concentration of excess ^{15}N per N in plant leaves and roots.

SI.1.5 Data quality control

We conducted a multistep hierarchical data-cleaning method (11) to provide quality control for the compiled data as follows:

First, soil property data and plant trait data were checked for improbable values, with the goal of excluding likely errors or measurements with incorrect units but without excluding true extreme values. We manually checked plant trait values and excluded only those that were obviously erroneous based on our expert knowledge of these species.

Second, for each case, identifying whether a given observation (x) was likely to be erroneous (that is, ‘error risk’) by calculating the difference between x and the mean (excluding x) of the taxon (species or site) and then dividing by the standard deviation of the taxon were conducted since the standard deviation of a trait value is related to the mean and sample size. We checked individual records against the entire distribution of the observations of trait data and removed any records with an error risk greater than 8 (that is, a value more than 8 standard deviations away from the soil property/plant trait mean value). For individual species across the sites, we estimated a species mean per location and removed observations for which the species (plot-

level) mean error risk was greater than 3 (that is, the species mean of that site was more than 3 standard deviations away from the species mean across all plots from the location).
Finally, we compared individual species records directly to the distribution of the values at the plot level. We excluded values above an error risk of 2.25.
After the above procedure was conducted, 124 data points (4.7%) were removed for soil properties, and 316 observations/data points (3.8%) were removed for plant traits.

In all cases, we visually checked the excluded values against the distribution of all observations for each species to ensure that our trait and soil property data cleaning protocol was reasonable. Furthermore, we found that 124 excluded data points (4.7%) were removed because soil properties were mainly based on the soil surface pH value (71%) and soil surface NO_3^- data (22%), and 316 data points were removed because plant traits were mainly based on the aboveground biomass of September (86%), which was caused by waste or the activity of small mammals, such as *Ochotona curzoniae.*

SI.1.6 Spatial autocorrection and uncertainty estimates

Because the plots included in this study were not uniformly dispersed over the Tibetan Plateau, we examined the potential of locations, such as locations TM, TGL, KXL and BLH, in relatively concentrated plots to drive the overall patterns. To do this, we first examined spatial autocorrelation in the trends in weather parameters, soil properties and plant traits using Moran's I in the R package lctools (12). Moran's I test results ranged from -1 to 1, where −1 indicates a perfectly dispersed variable, 0 indicates a randomly distributed variable, and 1 indicates that the data are perfectly autocorrelated. We observed that the results ranged from 0.001 to 0.018, which suggests that in this study, some variables were weak but had no significant spatial autocorrelation.
We conducted an analysis to compare trends, confidence intervals, and significance of trends over two time periods, 1995–2005 (n = 154) and 2006–2017 (n = 168), to assess whether different locations during observation years influenced the overall trends in active layer warming, active layer moisture, permafrost thawing, soil properties (0-50 cm, 50-100 cm, and 100-permafrost front), and plant traits we observed. For each time period, we used a subset of

locations that had data for at least 80% of the years within the defined time period. Following the established methods of ref. 13, we calculated a yearly anomaly in the active layer, soil properties, and plant traits for each location as the difference between each year's observation and the long-term mean. We then averaged these anomalies across all locations and used 1) the probability density function to test for a normal distribution and 2) linear regression to calculate the slope, significance, and confidence intervals of these averaged anomalies.

SI.1.7 Climate, permafrost dataset temporal assimilation and group split

To generate a dataset with consistent time scale (year) resolution within and among climate characteristics, soil properties, and plant traits, we extracted and averaged air temperature, total precipitation, soil temperature, and soil moisture for the growing season (from ^{1} May to ^{30} September) and nongrowing season (from ^{1} October to ^{30} April) at specific locations.

To directly compare the different effects of permafrost conditions on plant community traits under climate warming, we used the observed ALT time trends (from 1975 to 2017), and the 14 study locations were split into two groups. Group A consisted of TSH, QSH, SQH, GZ, MA, WQ, ZAD, XD, ZD, and HSX, with significantly positive increasing trends (ALT significantly increased with time under climate warming). Group B consisted of AD and BLH without significant changes and KXL and QML with significantly negative trends (ALT significantly decreased with time under climate warming). To test whether the split standard was not an artifact of our group method, we applied a control plot and fitted it by linear less squares. The slope was 85.88, the correlation coefficient (r^2) was 0.8, and p<0.01, which demonstrated the sensitivity of the changes in ALT in air temperatures.

SI.1.8 Characterizing trends in climate and permafrost

For each location, we calculated the mean ALT, mean soil temperature at 0-50 cm, mean soil temperature at 50-100 cm, mean soil moisture at 0-50 cm, and mean soil moisture at 50-100 cm in a given year for our defined growing season to obtain a mean annual value. These variables and the mean annual air temperature for each location were then used to calculate 1) the long-term trends for climate change, active layer warming, active layer moisture, and permafrost thawing and 2) group level (group A and group B) mean annual soil temperature at 0-50 cm, soil temperature at 50-100 cm, soil moisture at 0-50 cm, soil moisture at 50-100 cm and variation in ALT. The difference between group A and group B was tested by a *t test*, and the significance level was 0.05. All time intervals were calculated using the Mann–Kendall test (trend package, R 4.1). We excluded datasets that had < 10 years. The control plots that measures the rate of air temperature per decade (δ Tair/decade) and the rate of ALT per decade (δ ALT/decade) were used to assess the sensitivity of permafrost thawing to climate warming and fitted by the linear least-squares method. The significance level was $p < 0.05$, and the confidence level was 95%.

SI.1.9 Characterizing trends in soil properties and soil nutrition

We calculated the mean soil bulk density, SOC concentration, TN concentration, C/N, Cl^- concentration, NO_3^--N concentration, NH_4^+-N concentration, Na^+ concentration, Ca^+ concentration, and Mg^+ concentration. For each location, we calculated the mean of the above properties for soil profiles (0-50 cm, 50-100 cm, and 100 cm permafrost front) in a given year to obtain a mean annual value. The definition for the 100 cm permafrost front, as it is not possible to precisely judge or distinguish by eye in the field, was the 100 cm permafrost front soil core that included5~10 cm permafrost. Mean annual soil properties and soil nutrition were then used to calculate 1) the long-term trends for the 0-50 cm, 50-100 cm and 100 cm permafrost fronts and 2) the variation in soil properties and soil nutrition for group A and group B. The difference between group A and group B was tested by a *t test*, and the significance level was 0.05. All trends were calculated by linear regression, and the slope was estimated by the linear least-squares method. The significance level was $p < 0.05$, and the confidence level was 95%.

SI.1.10 Characterizing trends in plant traits

For each location, we calculated the mean plant coverage, aboveground biomass in September, root maximum length, mean plant height (September), and plant community species richness in a given year (in our defined growing season period) to obtain a mean annual value. These variables were then used to 1) calculate the long-term trends for individual locations and 2) calculate the group-level plant trait time trend for group A and group B. All trends were calculated using linear regression and fitted by the least-squares method; the significance level was $p < 0.05$, and the confidence level was 95%.

SI.1.11 Linkage between permafrost thawing and nitrogen release

At ambient sites, linear regression was used to identify 1) the nitrogen source that was the major contributor to the 50-100 cm NO_3^- concentration variation, as we hypothesized that 0–50 cm was a proxy for the nitrogen source from active layer warming and 93% SOC was attributed to the 0-50 cm and 100 cm permafrost front proxies for the nitrogen source from permafrost thawing, and 2) the relationship between the variation in the NO_3^- concentration within the active layer (0-50 cm, 50-100 cm, and 100-permafrost front) and permafrost thawing (variation in ALT). The r^2 and significance level were calculated by the least-squares method. The significance level was $p < 0.05$, and the confidence level was 95%.

To assess the robustness of the inferred enhancement in NO_3^- concentration within the active layer from permafrost thawing, we used a contour map to delineate the variation in nitrate concentration (NO_3^-) within the active layer with permafrost thawing change (variation in ALT) from 1995 to 2017 (SF 15; Surfer 12.0). Kriging was used to grid NO_3^- concentration data at 10 cm intervals within 0-500 cm during 1995 to 2007; x axis is year, y axis is depth of active layer, Z axis is NO_3^-, Z axis is linear, there is no transform and inflate conveys hull by 0.

SI.1.12 Causality analysis between maximum root length and nitrogen increase at 50-100 cm

To demonstrate the causal relationship between the maximum root length increase and the nitrogen concentration increase of 50-100 cm, we ran the causality test by convergent cross mapping with the rEDM package of R 4.1. The optimal value of the embedding dimension E was 2, estimated by the function of the SSR pred boot. Convergent cross mapping demonstrated that an increase in soil nitrogen of 50-100 cm caused the maximum root length change (increasing), and the time lag was approximately 2 years. This result was consistent with field observations of isotope ^{15}N where labeled N rejected to the front of permafrost could be taken up by the deep-rooted plant in two years. Furthermore, convergent cross mapping was used to improve our understanding of the relationship between climate change or permafrost thawing or active layer warming or active layer soil moisture and maximum root length. The results were assessed by the r^2 and p value, with a significance level <0.05.

SI.1.13 Multiple regression analysis of drivers of plant trait trends

We conducted a multiple regression analysis of the air temperature, total precipitation, active layer temperature, active layer moisture, variation in ALT, soil nitrogen variation within the active layer (variation in N-NO_3^- concentration and N-NH_4^+ concentration), and drivers of observed plant trait (maximum root length, species richness, and aboveground biomass in September) trends at each location. Predictors in the analysis included growing season air temperature, growing season total precipitation, growing season soil temperature of 0-50 cm, growing season soil temperature at 50-100 cm, growing season soil moisture at 0-50 cm, growing season soil moisture at 50-100 cm, growing season soil nitrogen (including N-NO_3^- and N-NH_4^+) at 0-50 cm, growing season soil nitrogen at 50-100 cm, growing season soil nitrogen at the 100 cm permafrost front, variation in ALT, nongrowing season air temperature, nongrowing season soil temperature at 0-50 cm, nongrowing season soil temperature at 50-100 cm, annual air temperature, annual soil temperature at 0-50 cm, and annual soil temperature at 50-100 cm.

All variables were standardized by Z-scores to facilitate a comparison of model coefficients across the variables with different units. Selection variables were entered stepwise. We verified that multicollinearity was not a problem by checking that the variance inflation factor was well below ten for all variables (14). We used the leaps R package to select subset models including all predictors and two-way interactions and selected the fitted model having the lowest Akaike information criterion (AIC). The results are described by the coefficient (r^2) and *p* value, and the significance level <0.05.

SI.1.14 **Structure equation model (SEM)**

Piecewise SEM was examined to identify 1) the pathway through which climate change potentially affects plant growth and 2) the difference between the direct and indirect effects of temperature, water balance and soil nutrition on plant growth. The mean value at the site level for the growing season was used in the SEM analysis and split into two groups, A and B (supplementary Fig. S1). Variables that only demonstrated a significant correlation ($p<0.05$) with plant traits in the multiple regression analysis were pooled into the SEM. Nutrition variation was represented by the nitrogen variation, whereas ammonium (NH_4^+) variation delineated the nitrogen released from the permafrost. Ultimately, 7 variables were used in the SEM.

All variables were standardized (mean zero, unit variance) using Z-scores. Then, principal component analysis (PCA) was used to summarize the structure between plant growth and driver parameters. We assumed linear Gaussian relationships between variables included in the model, which tested normality with density plots for each variable (15).

As plant uptake of nitrogen released from permafrost has a two-year time lag, the final climate change and plant trait dataset was from 1997 to 2017, and the soil nitrogen dataset was from 1995 to 2015. We fit separate models window-by-window from 0 to 5 years both for the growing season and nongrowing season to 1) test whether the time lag of 2 years in the SEM was not an artifact setting and 2) account for possible time lag effects of climate change variables (i.e., nongrowing season air temperature and soil temperature) and nitrogen released from the permafrost thawing front during plant aboveground senescence.

To examine pathways by which climate change potentially affects plant growth and to differentiate between direct and indirect effects of temperature (air temperature, growing degree days, soil temperature at 0-50 cm, soil temperature at 50-100 cm, and variation in ALT), water balance (soil moisture at 0-50 cm and soil moisture at 50-100 cm) and soil nutrition (N-NO_3^- and N-NH_4^+ concentration in that 0-50 cm, 50-100 cm, and 100 cm-permafrost front) on plant growth, we used piecewise SEMs.

Before the SEM analysis, all variables for the 14 locations were 1) split into two groups based on the variation in ALT under climate warming, and the details are presented in Supplementary Fig. S1 and 2) only demonstrated a significant correlation with plant traits (p<0.05) in the above multiple regression analysis and were pooled into the SEM. For each group of variables, the mean value at the level of location was used in SEM analysis. As the plant uptake of nitrogen released from permafrost has a two-year time lag, the final climate change and plant trait dataset was from 1997 to 2017, and the soil nitrogen dataset consisted was from 1995 to 2015. Then, we used maximum likelihood estimation to interpolate the deficiency of data (16). Considering regional climate and using a priori knowledge, we included only growing season climate variables in our SEM, and nongrowing season and annual climate variables were excluded from the analyses. Although plant growth relationships with dormant season climate are occasionally reported, this information was not included in the SEM analyses.

After the data were compiled, a conceptual model was constructed to investigate complex (i.e., direct and indirect) relationships among plant growth and temperature, water balance, and soil nitrogen of both groups of responders. Soil moisture at 0-100 cm was used as a surrogate for the water balance among precipitation, ice melt, unfrozen water, and evaporation in the model. Because the maximum root length ranged from 50 cm to 100 cm for group A, the soil moisture and soil temperature at 0-100 cm were both chosen. For group B, the maximum root length ranged from 0 cm to 50 cm, and the soil moisture and soil temperature both ranged from 0-50 cm. To explore the potential mechanisms behind plant growth responses associated with changes in temperature, moisture and nutrition, the same SEM structure variables were applied to groups A and B.

As the nitrogen variation was mainly caused by active layer warming and permafrost thawing, we grouped the variation in nitrogen into two parts: 1) one part was related to active layer warming, as the ammonium (NH_4^+) data were sampled from 2008 to 2017 and nitrate (NO_3^-) data were sampled from 1995 to 2017, the nitrate (NO_3^-) variation at 0-100 cm accounted for 73% of the total nitrogen variation at 0-100 cm, and to avoid the uncertainty in data weight, here only the nitrate (NO_3^-) concentration in the 0–100 cm (averaged by NO_3^- concentrations at 0–50 cm and 50–100 cm) layer was used for further analysis with the data on the ammonium (NH_4^+) concentration in the 0–100 cm layer being excluded; 2) the other part was related to permafrost thawing. NH_4^+ variation accounted for 93% of the nitrogen variation in the 100 cm permafrost front. To avoid uncertainty in data weight, only the ammonium (NH_4^+) variation was included to delineate the nitrogen released from permafrost.

In the end, 7 variables were used in the SEM: (1) the mean air temperature (MAT) during the plant growing season; (2) the mean soil water content at 0–100 cm (SWC; averaged by 0–50 and 50-100 cm) during the growing season; (3) growing degree days, which is a cumulative sum of daily air temperature above 0 °C; (4) active layer warming, which was proxied by the mean soil temperature of 0–100 cm (Tsoil; averaged by soil temperature at 0–50 and 50–100 cm) and NO_3^- concentration at 0–100 cm; (5) permafrost thawing, which was proxied by the maximum ALT and NH_4^+ concentration of the 100 cm–permafrost front; (6) plant growth, including aboveground biomass in September and species richness; and (7) the maximum length of roots, which was the maximum root depth.

To test whether the time lag (2 years) in the SEM was not an artifact and account for possible time lag effects of climate change variables (i.e., nongrowing season air temperature and soil temperature) and the nitrogen released from the permafrost thawing front when plants experienced aboveground senescence, we fit separate models window-by-window from 0 to 5 years both for the growing season and nongrowing season.

We then created an expression of community structure compatible with the SEM. We assumed linear Gaussian relationships between the variables included in the model that tested each variable for normality with density plots. All variables were standardized (mean zero, unit variance) using Z-scores. Then, PCA was used to summarize the structure between plant growth and climate drivers by FactoMineR packages of R 4.1. All variables were entered before SEM analysis to facilitate the interpretation of parameter estimates.

To test the goodness–of–fit of our SEMs, we used chi square (x^2), degrees of freedom (*d.f.)*, and the root-mean-square error of approximation (RMSEA; the model had a good fit when the RMSEA was indistinguishable from zero to 0.05). A path coefficient is analogous to the partial r^2 or regression weight and describes the strength and sign of the relationships between two variables (16). We calculated the standardized total effects of all drivers on the plant growth of active layer warming and permafrost thawing attributes. The net influence that one variable had upon another was calculated by summing all direct and indirect pathways (effects) between two variables. All SEM analyses were conducted using the piecewise SEM package of R 4.1.

SI.2 Figures and Tables

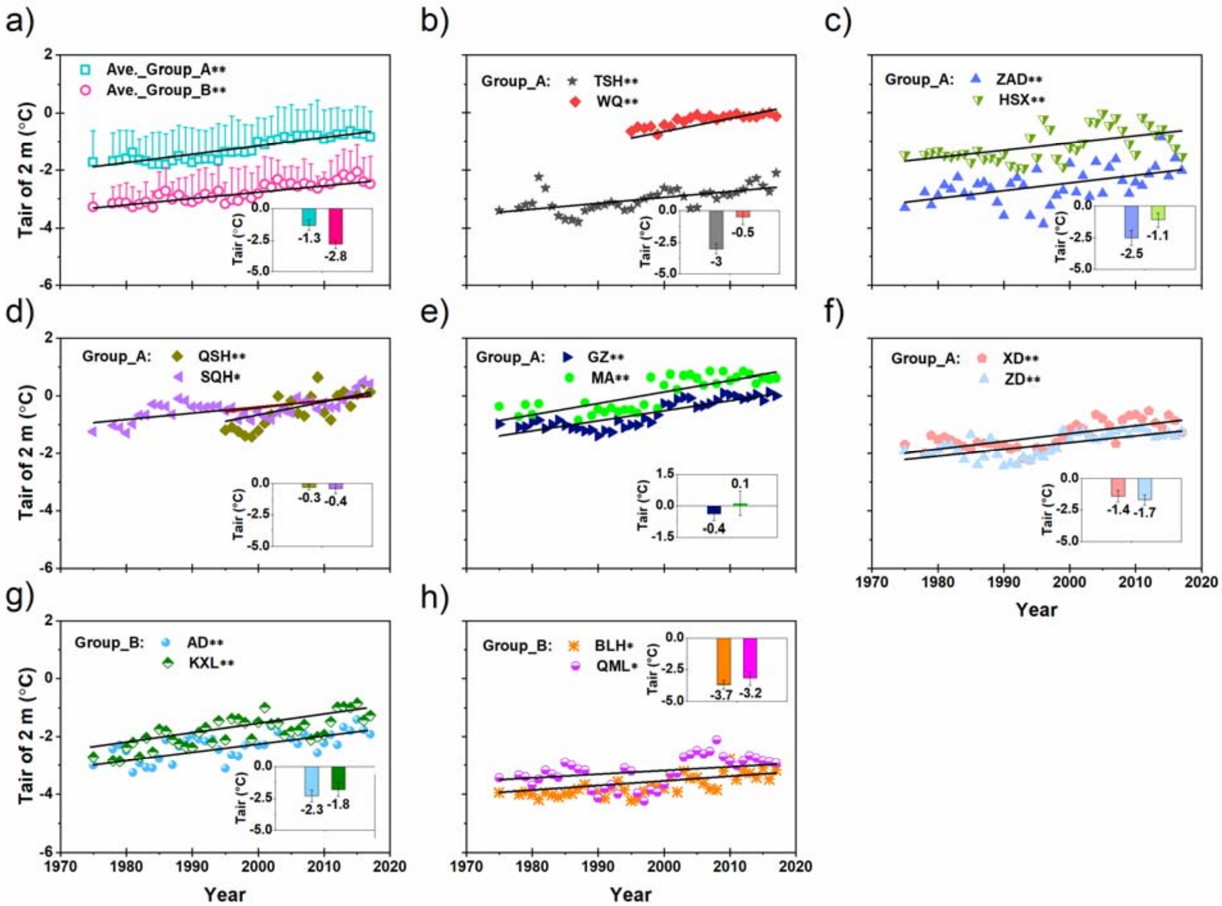

Supplementary Figure S1. Temporal changes in annual air temperature (Tair) at a height of 2 m (MAAT) on the Tibetan Plateau from 1975 to 2017. **a** is shown MAAT temporal changes for group A locations and group B locations from 1975 to 2017. For group A and B separation details, please see Supplementary Figure S1. Error bars denote SE, n = 8 for 1975–1994 and n = 10 for 1995–2017 for group A, and n=4 for group B. Subfigures **b**, **c**, **d**, **e)**, and **f** show the annual air temperature data of group A locations of TSH, WQ, ZAD, HSX, QSH, SQH, GZ, MA, XD, and ZD, respectively. Subfigures **g** and **h** show the annual air temperature data of group B locations of AD, KXL, and BLH, QML, respectively. Solid lines for 1975–2017 indicate significant changes ($p < 0.01$, **; $p < 0.05$, *). The insets show the mean annual air temperature (MAAT) for group A, group B and specific locations, which with different color columns from 1975 (locations WQ and QSH from 1995) to 2017.

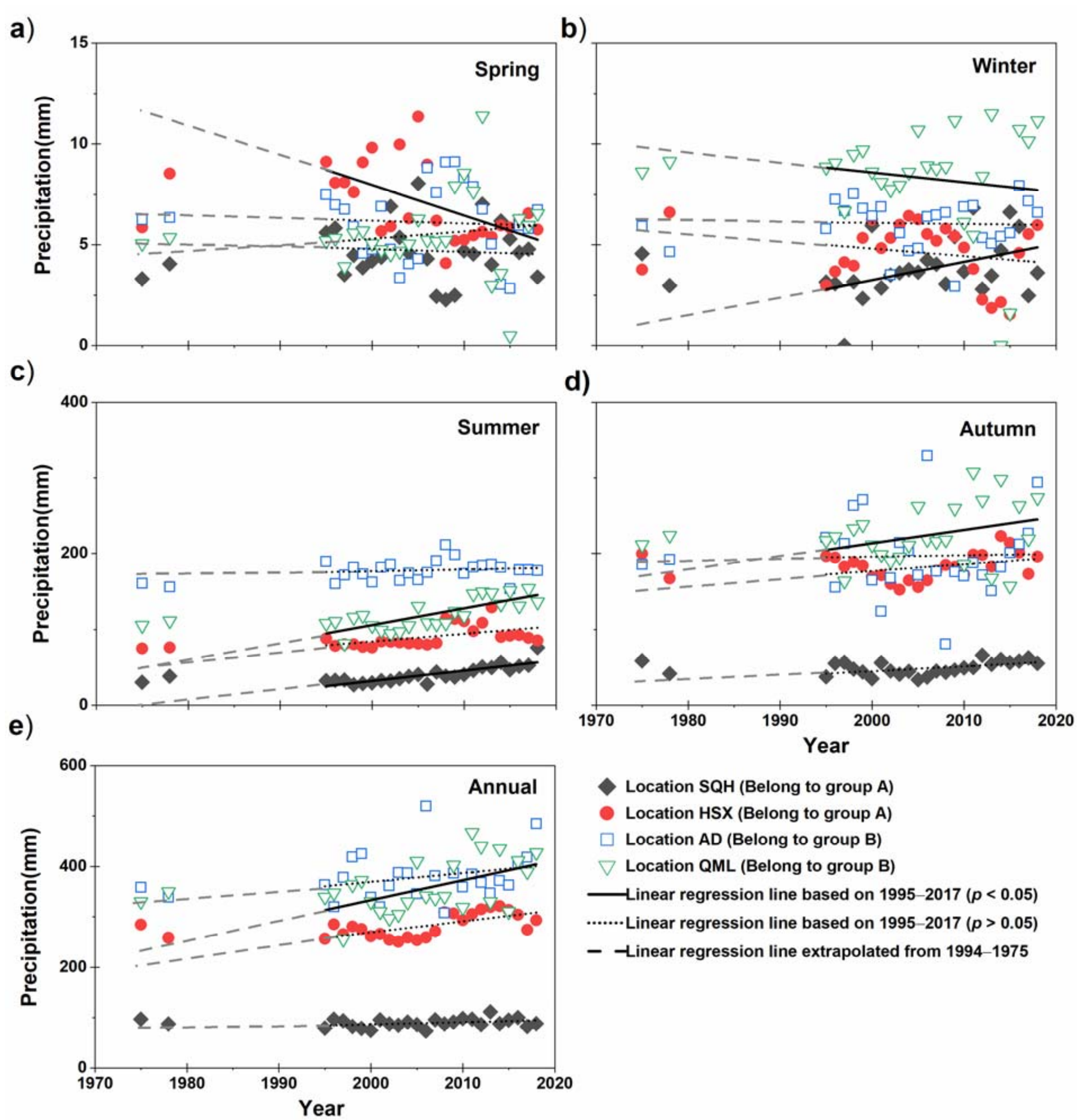

Supplementary Figure S2. Precipitation of 4 representative types of 14 locations (locations SQH and HSX belonged to the Group A; Locations AD and QML belonged to the Group B) in the permafrost region of the Tibetan Plateau from 1975 to 2017. Subfigure **a**, **b**, **c**, **d**, and **e** is used to designate spring, winter, summer, autumn, and annual total precipitation, respectively.

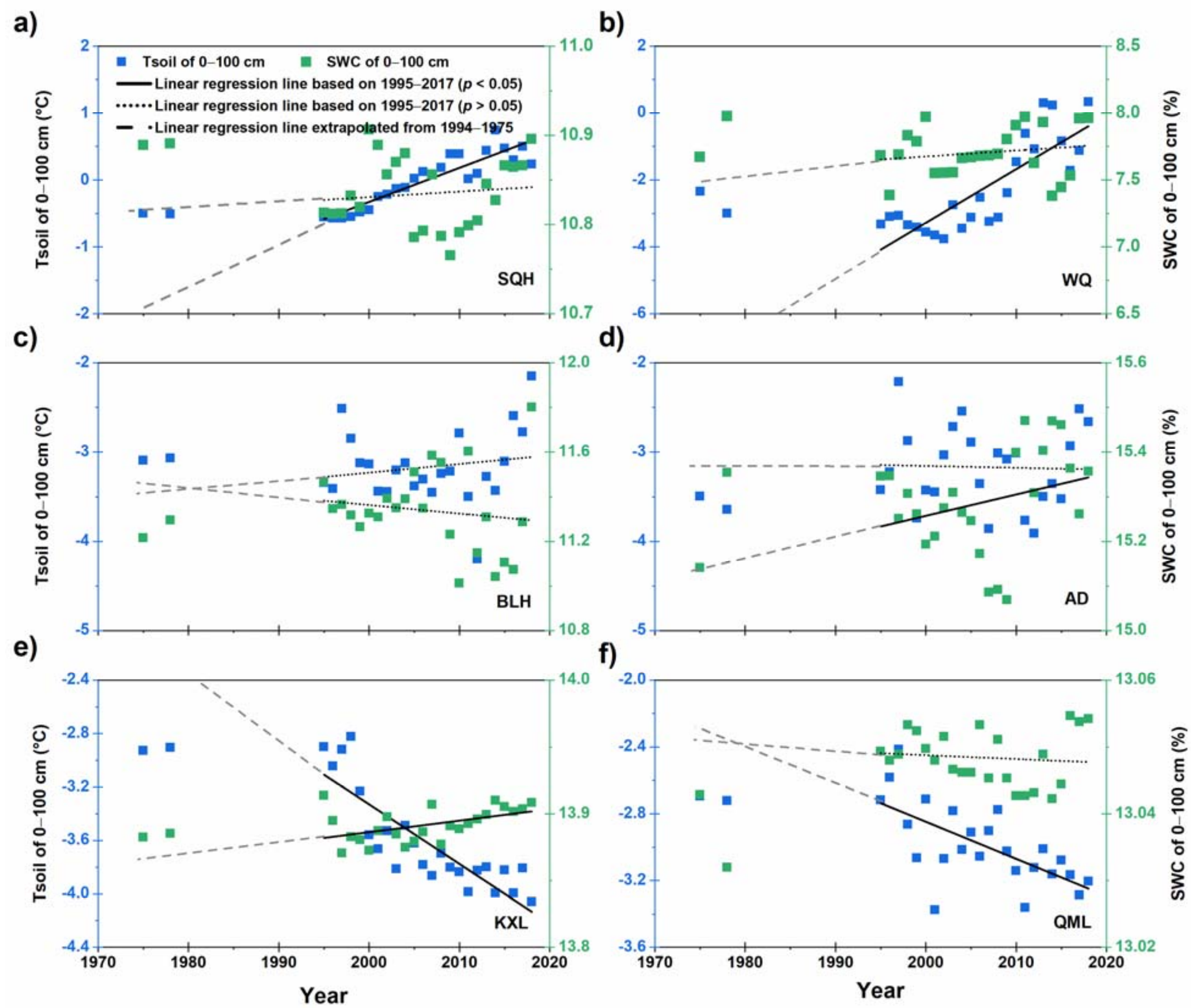

Supplementary Figure S3. Mean annual soil temperature (Tsoil) and soil water content (SWC) of 0–100 cm changes from 1975–2017 for six type locations on Tibetan plateau (Figs. S9 a-f). Location SQH, WQ belonged to group A; location BLH, AD, KXL, QML belonged to group B.

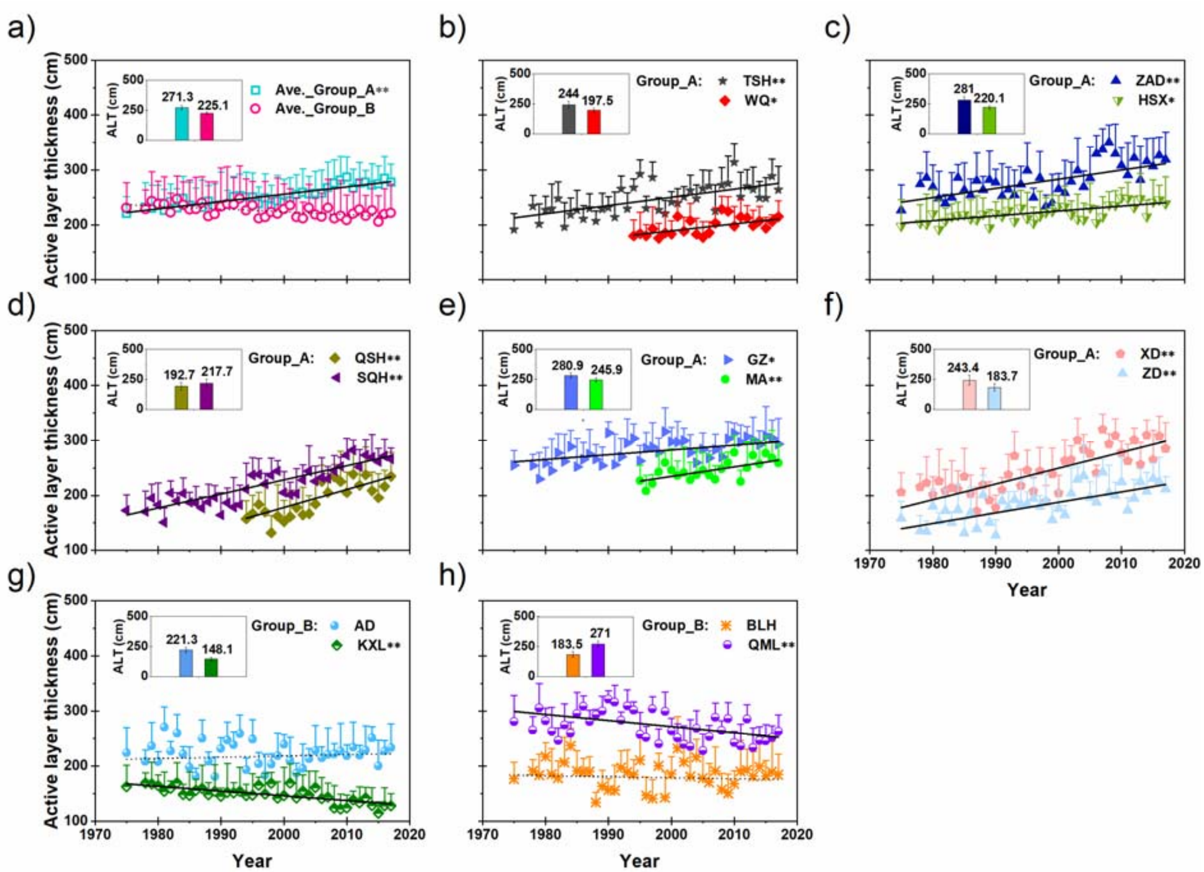

Supplementary Figure S4. Temporal changes in active layer thickness (ALT) on the Tibetan Plateau from 1975 to 2017. **a** is shown mean ALT temporal changes for group A locations and group B locations from 1975 to 2017. Error bars denote SE, n = 7 for 1975–1994 and n = 10 for 1995–2017 for group A, and n=4 for group B. Subfigures **b**, **c**, **d**, **e**, and **f** show the ALT data of group A locations of TSH, WQ, ZAD, HSX, QSH, SQH, GZ, MA, XD, and ZD, respectively. Subfigures **g)** and **h)** show the ALT data of group B locations of AD, KXL and BLH, QML, respectively. Solid lines for 1975–2017 indicate significant changes ($p < 0.01$, ** and $p < 0.05$, *), while dotted lines indicate non-significant changes ($p > 0.05$). The insets show the mean annual ALT for group A, group B and specific locations, which with different color columns from 1975 (locations WQ, QSH, and MA from 1995) to 2017.

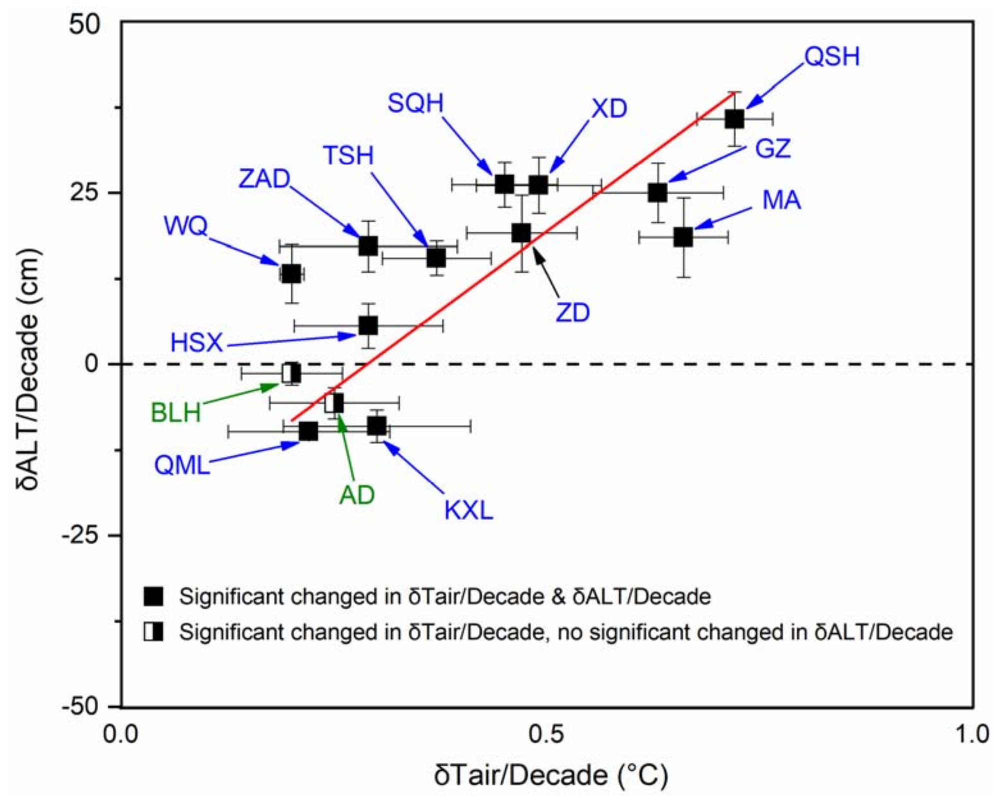

Supplementary Figure S5. Changes in air temperature and active layer thickness (ALT) per decade on the Tibetan Plateau from 1975 to 2017. Based on location-specific *t*-tests, the 14 stations are divided in group A locations (with a significant positive change in ALT with respect to air temperature; locations TSH, QSH, SQH, GZ, WQ, ZAD, XD, ZD, and HSX) and group B locations (with a significant negative in ALT with respect to air temperature, locations KXL and QML or no significant in ALT with respect to air temperature, locations AD and BLH). One standard deviation is shown as horizontal and vertical bars for δTair/decade (n = 4) and δALT/decade (n = 4), respectively. The red line is the linear fit line, which illustrates the sensitivity of changes in active layer thickness and changes in air temperatures ($y = 85.88X - 25.02$, r = 0.80; $p < 0.01$).

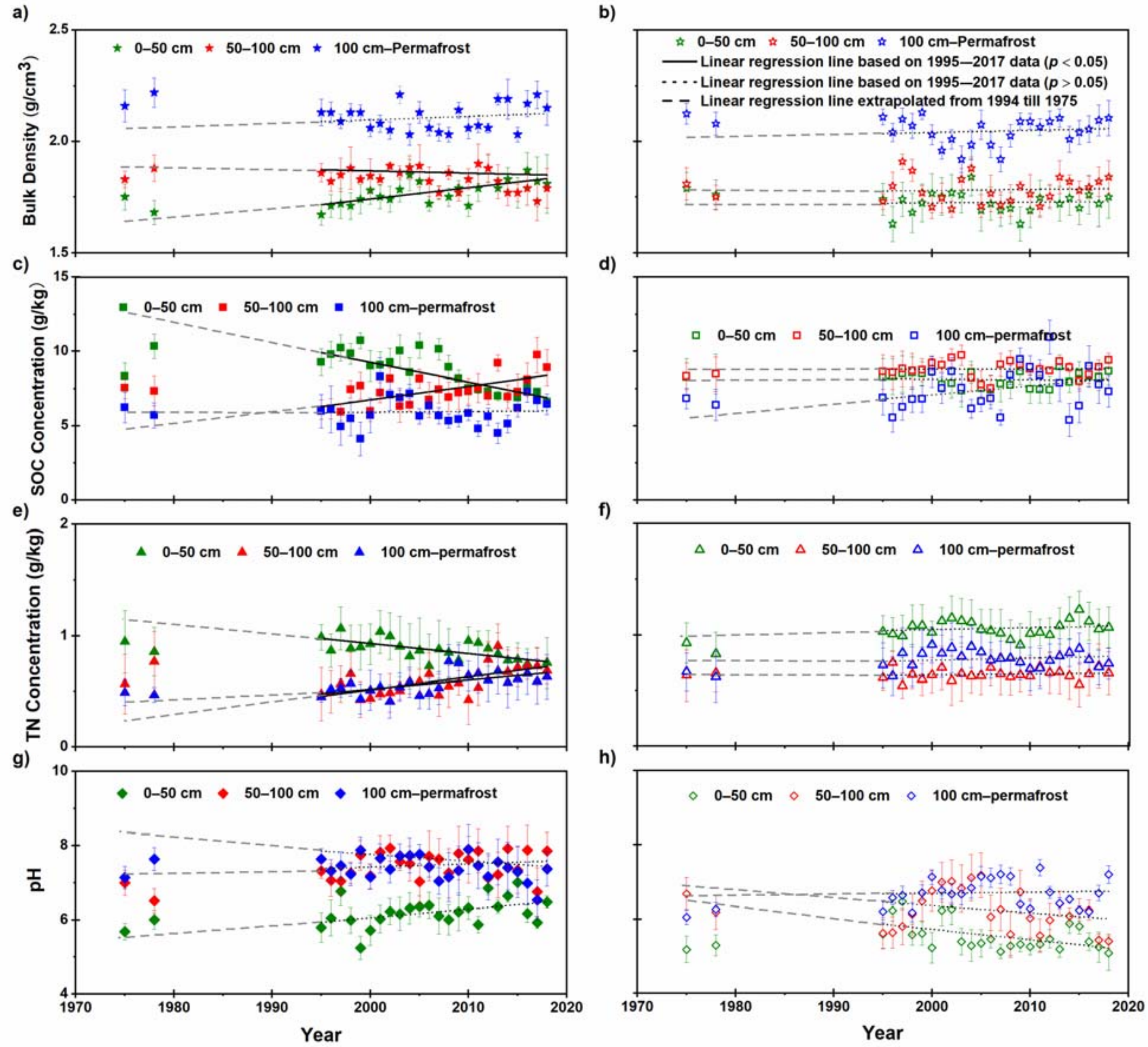

Supplementary Figure S6. Temporal changes in soil properties at three depth intervals averaged at locations across the Tibetan Plateau, which include soil bulk density, soil organic carbon (SOC) concentration, total nitrogen (TN) concentration, and soil pH. Average data are shown for group A locations (subfigures **a**, **c**, **e**, and **g**) and group B locations (subfigures **b**, **d**, **f** and **h**). Vertical bars represent one standard deviation, n = 6 for 1975, 1978, and n = 10 for 1995–2017 in group A; n =3 for 1975, 1978 and n =4 for 1995–2017 in group B.

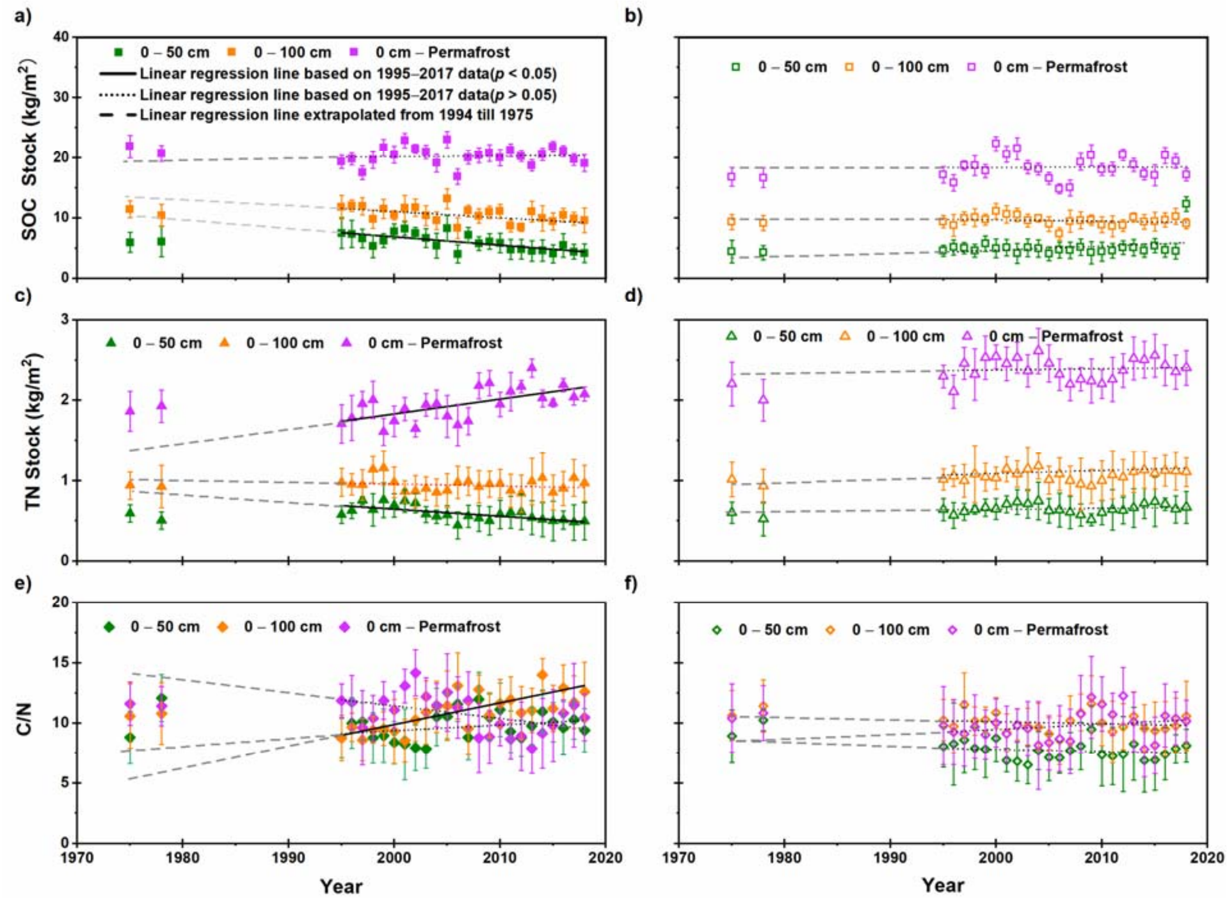

Supplementary Figure S7. Temporal changes in the soil organic carbon stock (SOC stock), total nitrogen stock (TN stock), and carbon–to–nitrogen ratio (C/N) at three depth intervals at locations across the Tibetan Plateau. Subfigures **a**, **c, and e** for group A locations; **b**, **d**, and **f** for group B locations. Worth notes, three depth intervals ware 0–50 cm, 0–100 cm, and 0 cm–permafrost. Vertical bars represent one standard deviation, n = 6 for 1975, 1978, and n = 10 for 1995–2017 in group A; n =3 for 1975, 1978 and n =4 for 1995–2017 in group B.

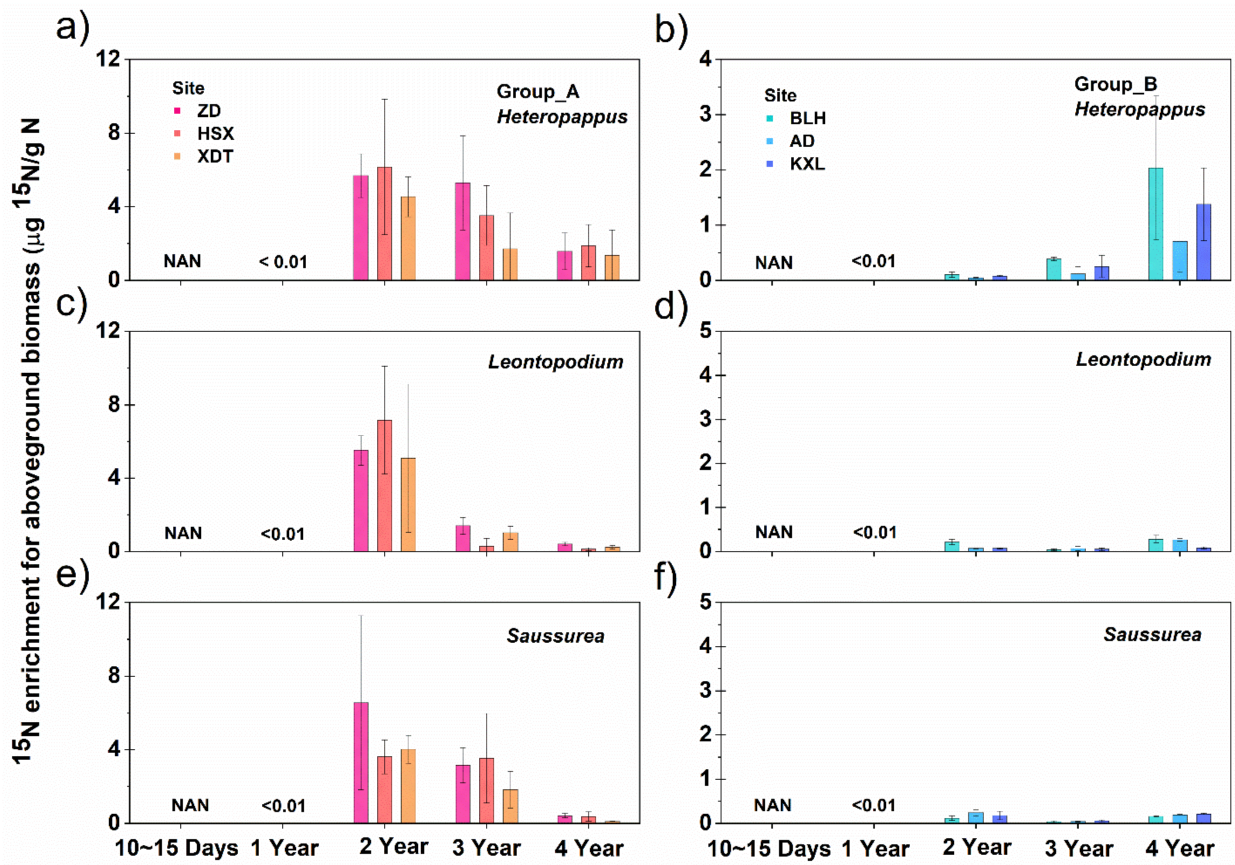

Supplementary Figure S8 Enrichment $^{15}N\_NH_4Cl$ in aboveground mass (including leaves and stem) of shallow-rooted species (average root length less than 20 cm) by treatment after 10~15days, 1 year, 2 years, 3 years, and 4 years for group A (**a**, **c**, **e**) and group B (**b**, **d**, **f**). **a** and **b** were *Heteropappus bowerii* (Hemsl.) Griers. (*Heteropappus*), **c** and **d** were *Leontopodium nanum (Hook. f. et Thoms.) Hand.-Ma* (*Leontopodium*), and **e** and **f** were Saussurea arenaria Maxim (*Saussurea*). vertical bars representing one standard deviation, n = 15, excluded the 1 year, n= 12.

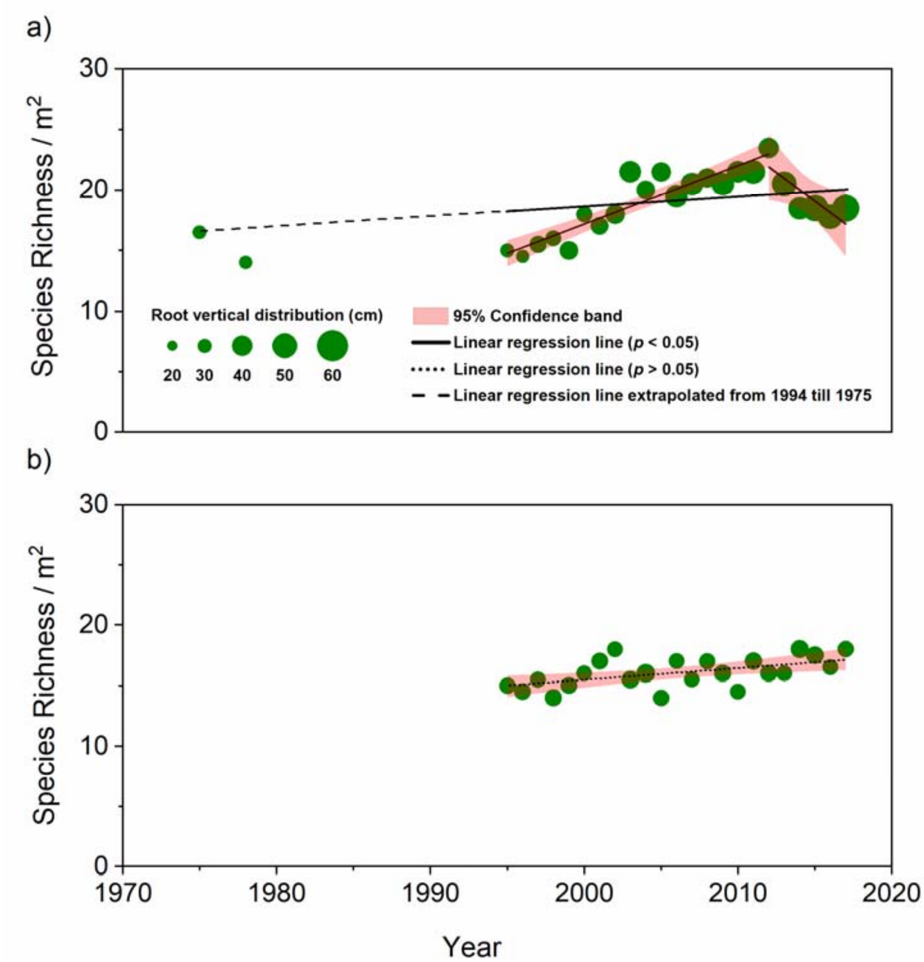

Supplementary Figure S9. Changes in specie richness and root vertical distribution from 1975 to 2017. The size of green dot indicates the difference of root vertical distribution. Subfigure **a** show the group A locations and **b** for the group B locations.

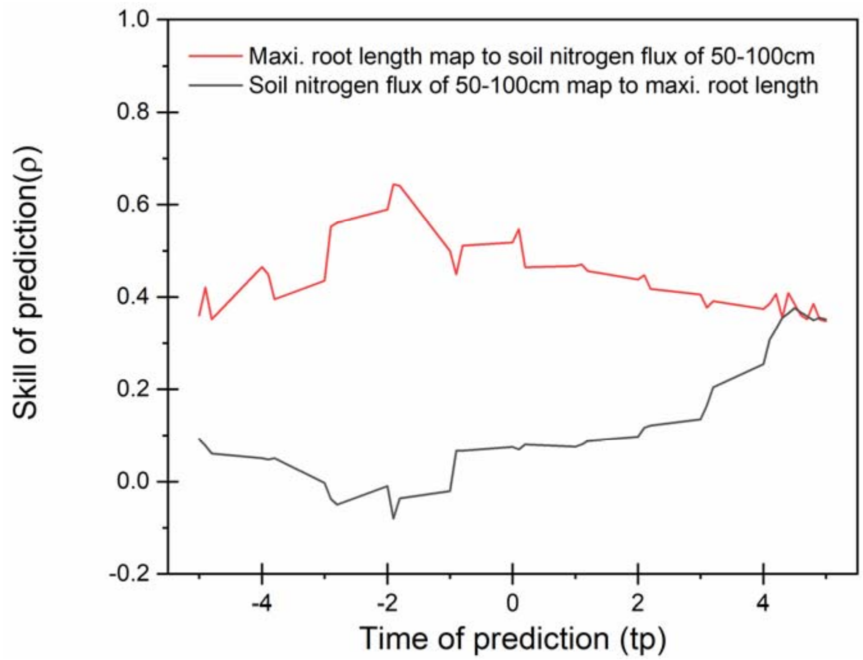

Supplementary Figure S10. Causality test running for the variation of root length map to soil nitrogen flux of 50-100 cm (red line) and soil nitrogen flux of 50-100 cm map to root length (grey line), respectively. Skill of prediction (ρ) for red line reaches the peak when time prediction (tp) around -2, demonstrate that the soil nitrogen flux of 50cm caused the root length change (increase), and the time lag is about 2 years. This result consisted with field observations of isotope ^{15}N that label N rejected to the front of permafrost is could be uptake by the deep-rooted plant in two years. In contrast, ρ of the grey line peak *arrived* maximum when tp around 4, which means the hypothesis of variation of root length caused soi nitrogen flux of 50cm variation is impossible. The optimal value of the embedding dimension E= 2, estimated by function of SSR pred boot (R).

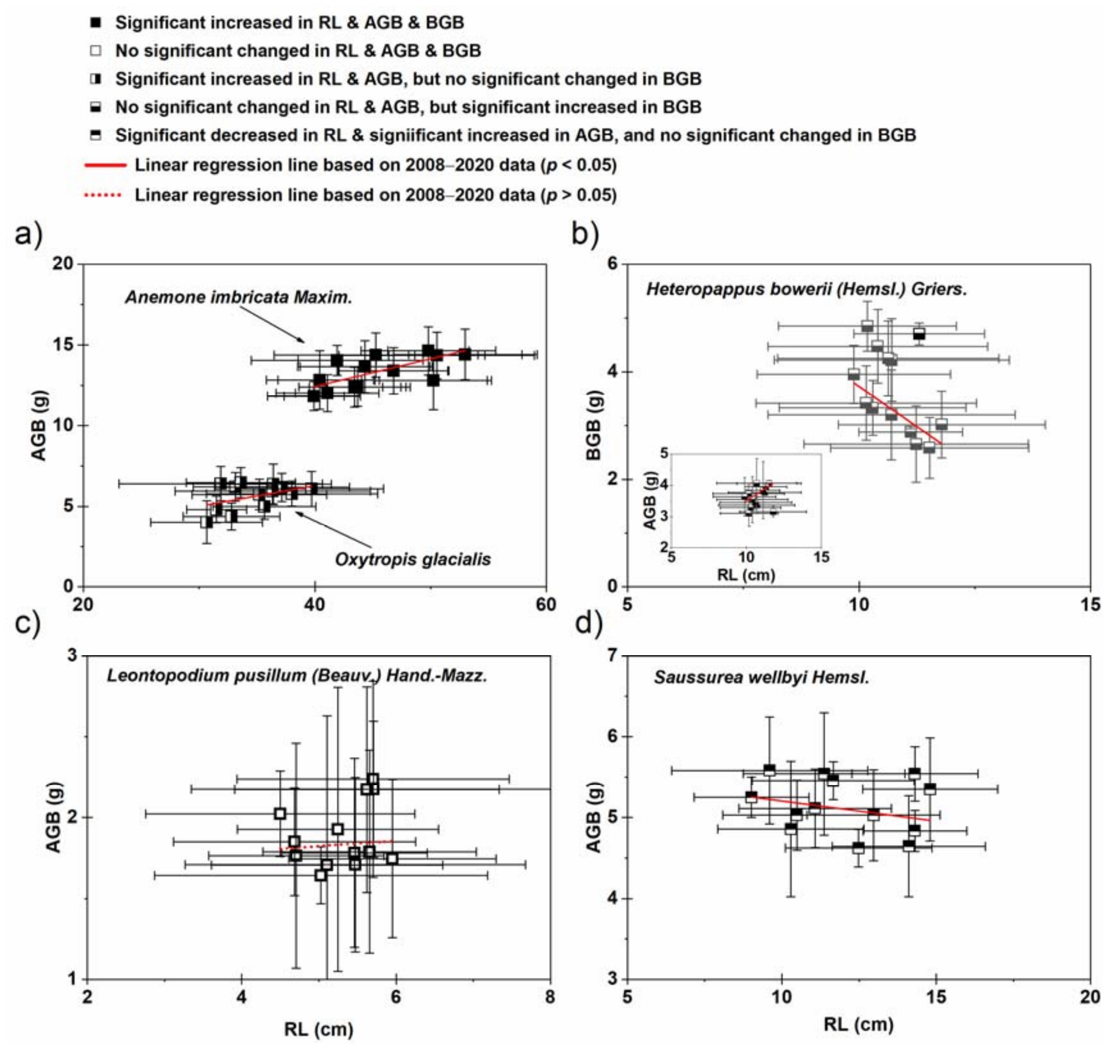

Supplementary Figure S11. Changes in root length (RL), aboveground biomass (AGB), and belowground biomass (BGB) for species type at the location XD (belonging for group A) from 2008 to 2020. **a** is two types deep-rooted species *Anemone imbricata* Maxim. and *Oxytropis glacialis*; **b**, **c**, and **d** are three shallow-rooted species *Leontopodium pusillum* (Beauv.) Hand.-Mazz., *Heteropappus bowerii* (Hemsl.) Griers., and *Saussurea wellbyi* Hemsl. **Worth note**, **b** is the changes in RL and BGB, the **inset** is the changes in RL and AGB for *Heteropappus bowerii* (Hemsl.) Griers. Vertical and horizontal bars represent one standard deviation, n = 4.

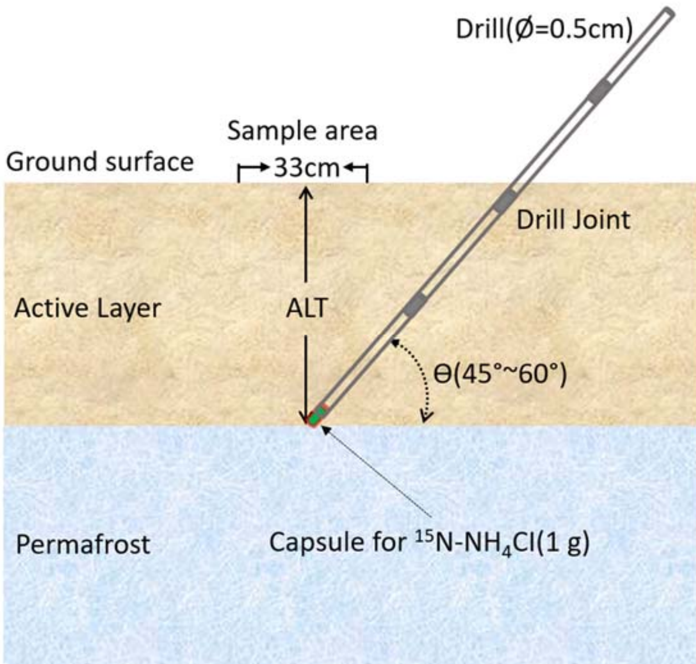

Supplementary Figure S12. Schematic of field experiment for $^{15}N-NH_4CI$ capsule rejection to the front of permafrost. Collection of plants were made only immediately above the rejection point. Tests have been made previous (11) to document that the method ensure that residue is not left at shallow depth which otherwise might be accessible for plant roots.

Supplementary Table ST1. Species abundance or species turnover (presence or absence) over time of group A.

No.	HP (cm)	RL (cm)	Year																								
			1975	1978	1995	1996	1997	1998	1999	2000	2001	2002	2003	2004	2005	2006	2007	2008	2009	2010	2011	2012	2013	2014	2015	2016	2017
1	27.4	37.2	√	√	√	√	√	√	√	√	√	√	√	√	√		√	√	√	√		√	√		√	√	√
2	27.4	38.2	√	√	√	√	√	√	√	√	√	√	√	√	√	√			√			√					
3	34.8	40.2	√	√	√	√	√	√	√	√	√	√	√	√	√	√				√	√	√	√				
4	26.5	33.5	√	√	√	√	√	√	√	√	√	√	√	√	√	√	√	√	√	√	√	√	√		√	√	
5	18.3	23.5	√	√	√		√	√		√	√		√	√	√								√	√			
6	15.4	18.5	√	√	√	√	√	√	√	√	√	√	√	√	√	√	√	√	√	√	√	√	√	√			
7	23.6	38.2	√	√	√	√	√	√	√	√	√	√	√	√	√		√	√	√								
8	6.5	14.0	√	√	√	√		√	√		√	√	√	√	√						√	√					
9	2.8	29.9	√	√	√	√	√	√	√	√	√	√	√	√					√	√							
10	1.8	23.7	√	√	√	√	√	√	√	√	√	√	√	√			√	√	√	√							
11	6.2	15.8	√	√	√	√	√	√	√	√		√		√		√				√							
12	8.0	14.6	√	√	√	√	√	√	√	√	√	√	√	√	√	√	√	√	√	√	√	√	√	√	√	√	√
13	5.9	5.1	√	√	√	√	√	√	√	√	√	√															
14	4.7	16.6	√	√	√	√		√			√		√		√								√		√		
15	8.1	11.4	√	√	√	√	√	√	√	√	√	√	√	√	√			√		√							
16	6.5	7.3	√	√			√	√	√	√	√	√															
17	6.8	13.8	√	√	√		√		√	√		√	√			√											
18	5.4	5.2	√	√	√	√	√	√	√	√	√	√		√	√				√								
19	11.1	12.1	√	√		√	√	√	√	√	√	√	√	√	√		√	√									
20	6.3	5.5	√	√	√	√					√			√		√											
21	9.8	10.8	√	√	√	√	√	√	√	√	√	√	√		√		√	√									
22	7.8	10.6	√	√	√	√	√	√	√	√	√	√	√	√	√	√	√	√	√		√		√	√	√		
23	5.7	5.1	√	√	√	√		√		√		√		√	√												
24	7.3	6.8	√	√	√	√	√	√		√	√	√		√		√	√	√									
25	6.4	6.2	√	√		√	√	√	√	√	√	√		√		√											
26	4.7	5.1	√	√	√		√		√	√	√		√														

27	5.1	6.1	√	√	√	√	√		√		√	√				√				√	√						
28	13.2	17.2	√	√	√	√	√	√	√	√	√	√	√	√	√	√	√		√	√	√						
29	18.6	39.2	√	√	√	√	√	√	√	√	√	√	√	√	√	√	√	√	√			√					
30	21.1	42.4	√	√	√	√	√	√	√	√	√	√	√	√	√	√	√	√	√	√	√	√	√	√	√	√	√
31	10.4	12.4	√	√	√	√	√		√	√		√	√														
32	7.6	12.3	√	√	√					√			√	√	√				√		√		√	√	√	√	√
33	12.9	10.0	√				√			√					√				√	√	√		√	√	√		√
34	15.7	8.3	√	√	√	√		√		√	√	√	√	√		√	√										
35	13.6	17.3	√	√	√		√	√	√	√	√	√	√	√	√	√		√									
36	15.6	42.8	√	√		√	√	√	√		√	√	√		√	√	√	√	√	√	√	√	√	√	√	√	√
37	6.9	33.3	√	√					√	√	√	√	√	√	√	√	√	√	√	√	√	√	√	√	√	√	√
38	25.7	43.6	√	√	√	√	√	√	√	√	√	√	√		√			√					√				√
39	16.8	13.5	√	√	√	√	√	√	√	√	√		√	√	√	√	√	√	√	√	√	√					
40	11.3	39.3	√	√	√	√	√	√	√	√	√			√					√		√				√		√
41	5.4	7.3	√	√	√	√	√	√	√	√		√			√	√		√	√	√	√	√	√	√	√	√	
42	12.6	42.4	√	√	√	√	√	√	√	√		√				√	√		√	√	√		√	√		√	√
43	8.4	31.1	√	√	√	√	√	√	√	√	√	√	√	√	√	√	√	√	√	√		√	√	√		√	
44	7.3	32.3	√	√	√	√		√			√	√			√		√		√								√
45	3.3	35.1	√	√	√	√	√	√	√	√	√	√	√			√		√	√	√	√	√	√				
46	13.4	42.5	√	√			√	√	√	√	√	√	√	√		√	√	√				√		√	√		√
47	11.1	15.2	√		√		√		√	√	√	√	√	√		√	√		√				√			√	√
48	17.7	38.3	√	√	√	√	√	√	√	√	√	√	√	√	√	√	√		√	√	√		√	√			
49	6.2	4.7	√	√		√	√	√	√	√	√	√	√		√	√				√	√	√	√	√	√	√	√
50	13.4	10.1	√	√	√	√					√	√	√	√	√	√	√				√		√	√	√	√	
51	24.2	42.3	√	√	√	√	√	√	√	√	√	√	√	√	√	√	√	√	√	√	√	√	√	√	√	√	√
52	12.6	12.1	√	√	√	√	√	√	√	√	√	√	√	√		√	√	√		√	√						
53	13.5	27.5	√		√	√		√		√		√	√	√					√								√
54	7.1	17.3	√	√	√	√	√	√		√	√	√	√	√	√	√	√	√	√	√	√	√	√	√	√	√	√
55	3.7	46.0	√	√		√	√	√	√	√	√	√	√	√	√	√	√	√	√	√	√	√	√	√	√		
56	16.8	42.3		√	√		√		√	√	√	√	√	√							√	√	√		√	√	√
57	35.1	47.2		√	√	√	√		√		√	√	√	√	√	√	√	√	√	√	√	√					
58	32.1	44.2		√	√	√	√	√	√	√	√		√	√	√	√	√	√	√					√			

59	23.6	45.2		√	√	√	√	√	√	√			√	√	√	√	√	√	√	√	√	√	√	√			
60	8.3	12.1			√	√	√	√	√	√			√	√	√		√		√		√	√	√	√	√	√	√
61	5.9	17.6			√	√	√		√	√			√	√	√	√		√	√	√	√	√	√	√	√	√	√
62	17.9	55.3											√	√	√	√			√	√	√	√	√	√	√	√	√
63	13.1	49.4											√	√		√	√	√	√	√	√	√	√	√	√	√	√
64	16.4	23.4											√	√		√	√	√	√	√		√	√		√	√	√
65	13.2	22.4												√				√		√		√	√	√	√	√	√
66	26.3	36.7													√			√		√		√		√	√	√	√
67	16.1	40.1													√	√	√	√	√	√	√	√	√	√	√	√	√
68	6.3	12.4													√	√		√		√	√	√	√		√	√	√
69	19.3	5.8													√	√	√	√	√	√	√	√	√	√	√	√	√
70	22.2	46.1													√	√	√	√	√	√	√	√	√	√	√	√	√
71	23.8	42.2														√	√	√	√	√	√	√	√	√	√	√	√
72	15.8	45.7														√	√	√	√	√	√	√	√				
73	6.0	41.3														√			√			√		√		√	√
74	15.7	50.3														√		√	√	√	√	√					
75	4.3	21.2														√	√	√		√	√			√	√	√	√
76	4.8	24.9															√	√		√	√	√			√	√	√
77	6.3	8.7															√	√				√		√	√	√	√
78	11.3	17.3															√	√	√	√	√	√	√	√	√	√	√
79	25.1	58.8															√	√	√	√	√	√	√	√	√	√	√
80	21.2	34.1															√		√				√	√		√	√
81	8.0	16.5																		√					√	√	√
82	4.3	24.6															√	√		√	√			√	√		√
83	5.0	6.0															√	√		√		√		√		√	
84	7.2	6.5															√	√		√	√	√	√	√	√	√	√
85	22.9	60.4																√	√	√	√	√	√	√	√	√	√
86	15.9	57.6																√	√	√	√	√	√	√	√	√	√
87	18.6	63.7																	√	√	√	√		√	√	√	√
Total			55	56	52	50	51	48	49	53	49	49	50	49	46	49	48	51	51	52	48	47	45	43	41	40	42

Note that HP is acronymic of mean height of plant, RL is acronymic of mean root length, values reported as annual means, not show the standard error. Species presence is used to designate √, species absence is used to designate blank, and No. is used to designate the species name. 1, *Kobresia littledalei* C. B. Clarke 2, *Kobresia tibetica* Maxim 3, *Kobresia robusta* Maxim 4, *Carex nudicarpa* (Y. C. Yang) S. R. Zhang (2015) 5, *Triglochin maritimum* 6, *Polygonum viviparum* L. 7, *Astragalus purdomii* 8, *Ranunculus longicaulis* C. A. Mey. var. *nephelogenes* (Edgew.) L.Liou 9, *Androsace tangulashanensis* Y. C. Yang et R. F. Hua. 10, *Androsace integra* (Maxim.) Hand－Mazz. 11, *Lagotis brachystachya* Maxim. 12, *Leontopodium pusillum* (Beauv.) Hand.-Mazz. 13, *Primula minor* Balf. f. et Ward 14, *Saussurea stella* Maxim. 15, *Aster alpinus* L. 16, *Thalictrum alpinum* L. 17, *Oxygraphis glacialis* (Fisch.) Bunge 18, *Saxifraga unguiculata* Engl. 19, *Taraxacum brevirostre* Hand.-Mazz. 20, *Silene gonosperma* 21, *Saussurea wellbyi Hemsl*. 22, *Polygonum sibiricum* Laxm. 23, *Gentianopsis paludosa* (Hook. f.) Ma 24, *Gentiana crenulatotruncata* (Marq.) T. N. Ho 25, *Gentiana futtereri* Diels et Gilg 26, *Glaux maritima* L. 27, *Callianthemum pimpinelloides* 28, *Heteropappus bowerii* (Hemsl.) Griers. 29, *Carex parvula* O. Yano 30, *Kobresia deasyi* C. B. Clarke 31, *Taraxacum tibetanum* Hand.-Mazz. 32, *Hedinia tibetica* (Thomson) Ostenf. 33, *Delphinium candelabrum* Ostf. var. *monanthum* (Hand.-Mazz.) W. T. Wang 34, *Delphinium candelabrum* Ostf. var. *monanthum* (Hand.–Mazz.) W. T. Wang 35, *Allium cyaneum Regel* 36, *Oxytropis pauciflora Bunge* 37, *Kobresia humilis* (C. A. Mey. ex Trautv.) *Sergiev* 38, *Iris potaninii* Maxim. 39, *Saussurea melanotrica* Hand.-Mazz. 40, *Erysimum chamaephyton* Maxim 41, *Parnassia trinervis* 42, *Corydalis dasyptera* Maxim. 43, *Potentilla multicaulis* Bge. 44, *Potentilla saundersiana* 45, *Arenaria brevipetala* Y. W. Tsui et L. H. Zhou. 46, *Aconitum tanguticum* (Maxim.) *Stapf* 47, *Dimor phost emon landulosus* Kar.et Kir 48, *Potentilla bifurca* 49, *Ajania tibetica* 50, *Aster flaccidus* Bge. subsp. *glandulosus* (Keissl.) Onno 51, *Pedicularis cheilanthifolia* 52, *Cremanthodium humile* 53, *Cortiella caespitosa* Shan et Sheh 54, *Ajania khartensis* 55, *Thylacospermum* Fenzl T. rupifragum Schrenk. 56, *Ceratoides compacta* (Losinsk.) Tsien et C. G. Ma 57, *Rheum moorcroftianum* Royle 58, *Rhodiola algida* (Ledeb.) Fisch. et Mey. 59, *Rhodiola quadrifida* 60, *Heraeleummillefolium* 61, *Polygonum sibiricum* Laxm. var. *thomsonii* Meisn. Ex 62, *Potentilla parvifolia* Fisch. ex. Lehm. 63, *Myricaria prostrata* Hook. f. et Thoms. ex Benth. 64, *Oxytropis glacialis* 65, *Poa litwinowiana* Ovcz. 66, *Elymus nutans* Griseb. 67, *Stipa purpurea* 68, *Dracocephalum heterophyllum Benth* 69, *Allium carolinianum*

DC. 70, *Carex orbicularinucis* 71, *Carex moorcroftii* Falc．Ex Boott 72, *Meconopsis horridula* Hook. f. et Thoms. 73, *Anemone imbricata* Maxim. 74, *Microula tibetica* 75, *Sibbaldia adpressa* 76, *Pleurospermum hedinii* 77, *Saussurea tibetica* C. Winkl 78, *Saussurea Arenaria* 79, *Oxytropis melanocalyx Bunge* 80, *Trisetum spicatum* 81, *Trisetum tibeticum* P. C. Kuo et Z. L. Wu 82, *Carex capillifolia* (Decne.) S. R. Zhang 83, *Draba altaica* (C. A. Mey.) Bunge 84, *Hypecoum erectum* L. 85, *Stipa roborowskyi* Roshev 86, *Oxytropis stracheyana* Benth. *ex* Baker 87, *Astragalus melanostachys*.

545 **Supplementary Table ST2. Species abundance or species turnover (presence or absence) over time of group B.**

			Year																								
No.	HP (cm)	RL (cm)	1975	1978	1995	1996	1997	1998	1999	2000	2001	2002	2003	2004	2005	2006	2007	2008	2009	2010	2011	2012	2013	2014	2015	2016	2017
1	30.8	37.8	√	√	√	√	√	√	√	√	√	√	√	√	√	√	√	√	√	√	√	√	√	√	√	√	√
2	29.3	37.0	√	√	√	√	√	√	√	√	√	√	√	√	√	√	√	√	√	√	√	√	√	√	√	√	√
3	37.7	37.2	√	√	√	√	√	√	√	√	√	√	√	√	√	√	√	√	√	√	√	√	√	√	√	√	√
4	29.7	31.6	√	√	√	√	√	√	√	√	√	√	√	√	√	√	√	√	√	√	√	√	√	√	√	√	√
5	22.3	23.0	√	√	√	√	√		√	√	√		√	√	√		√	√	√	√		√	√	√	√	√	√
7	26.6	33.5	√	√	√	√	√	√	√	√	√	√	√	√	√	√	√	√	√	√	√	√	√	√	√	√	√
8	11.4	14.7	√	√	√	√	√	√	√	√	√	√	√	√	√	√	√	√	√	√	√	√	√	√	√	√	√
9	8.3	28.9	√	√	√	√	√	√	√	√	√	√	√	√	√	√	√	√	√	√	√	√	√	√	√	√	√
10	6.1	25.6	√	√	√	√	√	√	√	√	√	√	√	√	√	√	√	√	√	√	√	√	√	√	√	√	√
12	13.2	16.1	√	√	√	√	√	√	√	√	√	√	√	√	√	√	√	√	√	√	√	√	√	√	√	√	√
13	9.8	9.9	√	√	√	√	√	√	√	√	√	√			√	√	√	√	√	√	√	√	√	√	√	√	√
15	12.4	12.0	√	√	√	√	√	√	√	√	√	√	√	√	√	√	√	√	√	√	√	√	√	√	√	√	√
16	10.4	8.2	√			√					√	√					√							√	√	√	√
17	10.8	15.0	√	√	√	√	√	√	√	√	√	√	√	√	√	√	√	√	√	√	√	√	√	√	√	√	√
18	10.4	9.4	√																				√				
19	15.9	16.0	√	√	√	√	√	√	√	√	√	√	√	√	√	√	√	√	√	√	√	√	√	√	√	√	√
20	12.3	8.1	√							√	√										√						
21	12.9	13.8	√	√	√	√	√	√	√	√	√	√	√	√	√	√	√	√	√	√	√	√	√	√	√	√	√
23	8.4	8.7	√	√		√	√		√	√	√		√	√	√	√		√		√	√	√	√	√		√	√
24	9.9	8.7	√	√	√	√																					
25	10.7	6.8	√	√	√	√	√	√	√																	√	√
26	12.1	6.4	√				√		√		√	√	√	√		√	√	√	√		√	√	√		√	√	
27	13.0	8.3	√	√	√	√	√	√	√	√	√	√	√	√	√	√	√	√	√	√	√	√	√	√	√	√	√
29	23.8	37.5	√	√	√	√	√	√	√	√	√	√	√	√	√	√	√	√	√	√	√	√	√	√	√	√	√
30	26.8	38.2	√	√	√	√	√	√	√	√	√	√	√	√	√	√	√	√	√	√	√	√	√	√	√	√	√

31	17.6	14.2	√		√	√		√	√		√	√		√	√	√											
65	19.9	22.8	√	√	√	√	√	√	√	√	√	√	√	√	√	√	√	√	√	√	√	√	√	√		√	
67	22.5	37.2	√	√	√	√	√	√	√	√	√	√	√	√	√	√	√	√	√	√	√	√	√	√	√	√	√
72	22.3	43.1	√								√			√		√	√	√			√	√	√				
73	12.0	38.1	√	√	√	√	√	√	√	√	√	√	√	√	√	√	√	√	√	√	√	√		√		√	√
76	10.1	23.9	√	√	√	√	√	√	√	√	√	√	√	√	√	√	√	√	√	√	√	√			√	√	√
77	11.2	11.2			√	√	√	√	√	√	√	√	√	√	√	√	√	√	√	√	√	√		√			
78	17.5	18.2			√	√	√	√	√	√	√	√	√	√	√	√	√	√	√	√	√	√	√	√	√	√	√
63	19.8	44.0			√			√	√				√		√	√	√	√	√	√	√	√	√			√	√
Total			31	25	28	29	27	26	29	26	30	26	26	27	27	28	28	28	26	26	28	28	26	25	23	28	26

Note that HP is acronymic of mean height of plant, RL is acronymic of mean root length, species presence is used to designate √, species absence is used to designate blank, and No. is used to designate the species name. The species name list same like supplementary table 1.

Supplementary Table ST3. Mean aboveground biomass for September (Biomass of Aboveground), mean plant coverage, and mean ratio of maximum root depth to the thickness of the active layer (Max root depth: ALT) for groups A (G–A) and B (G–B) over time.

Year	Biomass of aboveground (g/m^2)		Plant coverage (%)		Ratio of max. root depth and ALT		n	
	G–A	G–B	G–A	G–B	G–A	G–B	G–A	G–B
1975	NA	NA	> 60	> 65	0.11 ± 0.09	0.14 ± 0.2	52	27
1978	NA	NA	> 60	> 65	0.10 ± 0.07	0.14 ± 0.19	48	20
1995	237.7 ± 8.5	250.4 ± 8.5	68.2 ± 5.8	75.4 ± 5.5	0.09 ± 0.05	0.15 ± 0.18	59	22
1996	241.9 ± 9.0	249.8 ± 9.7	69.8 ± 5.5	79.3 ± 7.4	0.08 ± 0.03	0.16 ± 0.18	55	23
1997	231.3 ± 9.4	251.9 ± 10.2	63.3 ± 5.6	61.8 ± 6.9	0.09 ± 0.01	0.18 ± 0.17	50	25
1998	243.6 ± 9.7	247.6 ± 10.4	63.8 ± 6.2	61.3 ± 4.0	0.08 ± 0.01	0.15 ± 0.16	45	29
1999	243.6 ± 9.6	245.7 ± 10.0	73.3 ± 5.5	65.3 ± 6.0	0.09 ± 0.02	0.15 ± 0.16	79	31
2000	237.7 ± 8.7	246.2 ± 8.5	70.8 ± 5.2	79.7 ± 7.5	0.07 ± 0.02	0.15 ± 0.15	74	31
2001	245.7 ± 8.2	248.1 ± 7.9	69.1 ± 6.3	69.5 ± 8.2	0.09 ± 0.03	0.15 ± 0.15	69	29
2002	249.9 ± 7.	248.9 ± 7.4	65.2 ± 6.4	67.2 ± 5.6	0.09 ± 0.04	0.19 ± 0.14	64	30
2003	232.8 ± 7.8	252.7 ± 8.3	67.0 ± 5.5	57.1 ± 4.9	0.10 ± 0.05	0.24 ± 0.13	60	33
2004	241.2 ± 8.7	253.4 ± 9.6	67.8 ± 6.7	59.9 ± 6.9	0.08 ± 0.06	0.18 ± 0.12	78	34
2005	238.1 ± 9.1	252.7 ± 10	56.6 ± 7.4	63.1 ± 6.2	0.10 ± 0.07	0.21 ± 0.12	74	37
2006	236.0 ± 9.	253.7 ± 10.1	69.3 ± 6.3	54.2 ± 5.3	0.10 ± 0.08	0.18 ± 0.11	70	39
2007	235.7 ± 9.2	254.6 ± 9.7	73.8 ± 5.6	56.8 ± 6.8	0.11 ± 0.04	0.19 ± 0.10	66	20
2008	239.5 ± 9.4	254.4 ± 10.1	65.7 ± 5.6	53.7 ± 7.8	0.09 ± 0.02	0.21 ± 0.17	62	24
2009	228.3 ± 9.2	252.4 ± 9.6	58.7 ± 6.2	61.7 ± 8.6	0.11 ± 0.00	0.21 ± 0.17	51	28
2010	233.2 ± 8.8	249.5 ± 8.9	59.6 ± 4.1	64.4 ± 8.0	0.09 ± 0.03	0.16 ± 0.16	53	30
2011	221.0 ± 8.6	244.4 ± 9.1	54.4 ± 5.4	69.1 ± 6.3	0.12 ± 0.05	0.16 ± 0.15	52	33
2012	219.8 ± 8.8	233.4 ± 9.3	65.6 ± 7.0	63.1 ± 7.7	0.10 ± 0.04	0.17 ± 0.15	53	33
2013	227.8 ± 8.8	247.5 ± 9.3	63.2 ± 5.9	62.4 ± 9.3	0.11 ± 0.03	0.18 ± 0.14	63	34
2014	223.8 ± 9.2	229.4 ± 10.0	68.0 ± 5.8	74.3 ± 10	0.11 ± 0.03	0.16 ± 0.14	69	38
2015	229.0 ± 9.4	261.5 ± 9.9	64.7 ± 6.8	66.3 ± 6.6	0.12 ± 0.02	0.18 ± 0.13	57	36
2016	237.5 ± 8.6	256.5 ± 8.5	69.1 ± 5.2	67.6 ± 7.6	0.13 ± 0.02	0.20 ± 0.13	52	33
2017	233.8 ± 7.1	251.5 ± 8.6	70.1 ± 6.4	65.4 ± 7.1	0.12 ± 0.02	0.17 ± 0.12	50	35

Note: values reported as annual mean ± SE. Data of the thickness of the active layer (ALT) during 1975-1995 based on the re-analysis from air temperature (ref. 17), during 1996-2017 based on borehole soil temperature (method by ref. 5).

Supplementary Reference

1. Ding, L., Zhou, J., Zhang, X., Liu, S., & Cao, R., A long-term 0.01° surface air temperature dataset of Tibetan Plateau. *Data in brief*, *20*, 748-752(2018). https://doi.org/10.1016/j.dib.2018.08.107
2. Du Y., Data of climatic factors of annual average temperature in the Xizang (1990–2015). National Tibetan Plateau Data Center, (2019). https://data.tpdc.ac.cn/en/data/a46b446e-12ac-4ba3-b0b9-1ec6195d2aa8/?q=Data%20of%20climatic%20factors%20of%20annual%20average%20temperature%20in%20the%20Xizang
3. Falge, E., et al., Gap filling strategies for long term energy flux data sets. *Agric. For. Meteorol.*, 107(1), 71-77(2001). https://doi.org/10.1016/S0168-1923(00)00235-5
4. Dengel, S., et al., Testing the applicability of neural networks as a gap-filling method using CH 4 flux data from high latitude wetlands. *Biogeosciences*, 10(12), 8185-8200. (2013). https://doi.org/10.5194/bg-10-8185-2013
5. Wu, Q., & Zhang, T., Changes in active layer thickness over the Qinghai-Tibetan Plateau from 1995 to 2007. *J. Geophys. Res. Atmos.*, *115*(D9) (2010). https://doi.org/10.1029/2009JD012974
6. Krinner, G., et al., A dynamic global vegetation model for studies of the coupled atmosphere-biosphere system. *Global Biogeochem. Cycles*, *19*(1) (2005). https://doi.org/10.1029/2003GB002199
7. Bjorkman, A. D., et al., Plant functional trait change across a warming tundra biome. Nat., 562(7725), 57-62(2018). https://doi.org/10.1038/s41586-018-0563-7
8. Shaoling, W., Huijun, J., Shuxun, L., & Lin, Z., Permafrost degradation on the Qinghai–Tibet Plateau and its environmental impacts. *Permafr. Periglac. Processes*, 11(1), 43-53 (2000). https://doi.org/10.1002/(SICI)1099-1530(200001/03)11:1<43::AID-PPP332>3.0.CO;2-H

9. Yun, H., et al., Consumption of atmospheric methane by the Qinghai–Tibet Plateau alpine steppe ecosystem. *Cryosphere*, *12*(9), 2803-2819 (2018). https://doi.org/10.5194/tc-12-2803-2018
10. Wu, X., et al., Environmental controls on soil organic carbon and nitrogen stocks in the high-altitude arid western Qinghai-Tibetan Plateau permafrost region. *J. Geophys. Res. Biogeosci.*, *121*(1), 176-187(2016). https://doi.org/10.1002/2015JG003138
11. Essington, T. E., Introduction to Quantitative Ecology: Mathematical and Statistical Modelling for Beginners. Oxford University Press (2021).
12. Kalogirou, S., Destination choice of athenians: An application of geographically weighted versions of standard and zero inflated p oisson spatial interaction models. *Geographical Analysis*, *48*(2), 191-230(2016). https://doi.org/10.1111/gean.12092
13. O'Reilly, M., & Kiyimba, N., Advanced qualitative research: A guide to using theory. London, United Kingdom: Sage (2015). http://hdl.handle.net/10034/620998
14. Queen, J. P., Quinn, G. P., & Keough, M. J., Experimental design and data analysis for biologists. Cambridge university press (2002).
15. Grace, J. B., Structural equation modeling and natural systems. Cambridge University Press (2006).
16. Mallet, A. A., A maximum likelihood estimation method for random coefficient regression models. Biometrika, 73(3), 645-656(1986). https://doi.org/10.1093/biomet/73.3.645
17. Zou, D., et al., A new map of permafrost distribution on the Tibetan Plateau. Cryosphere, 11(6), 2527-2542(2017). https://doi.org/10.5194/tc-11-2527-2017